Showcasing research from Prof. Mingxian Liu's laboratory, School of Chemical Science and Engineering, Tongji University, Shanghai, China.

Versatile carbon superstructures for energy storage

The design strategies and underlying mechanisms of versatile carbon superstructures for energy storage are reviewed. Current challenges and development roadmaps have been proposed to spur further exploration of carbon superstructures.

As featured in:

See Lihua Gan, Mingxian Liu *et al.*, *J. Mater. Chem. A,* 2023, **11**, 12434.

ROYAL SOCIETY OF CHEMISTRY

rsc.li/materials-a

Registered charity number: 207890

Journal of Materials Chemistry A

ROYAL SOCIETY OF CHEMISTRY

REVIEW

View Article Online
View Journal | View Issue

Cite this: J. Mater. Chem. A, 2023, 11, 12434

Versatile carbon superstructures for energy storage

Ziyang Song,[a] Ling Miao,[a] Yaokang Lv,[b] Lihua Gan *[a] and Mingxian Liu *[a]

Received 28th November 2022
Accepted 29th January 2023

DOI: 10.1039/d2ta09258a

rsc.li/materials-a

Three-dimensional carbon superstructures with ingenious topographies and favorable functionalities present attractive prospects in energy fields. Compared to the simple low-dimensional segments (*e.g.*, nanosheets, nanoparticles), carbon superstructures deliver excellent skeleton robustness, more uncovered electroactive motifs, and superior reaction kinetics, which are particularly useful for electrochemical energy storage. Therefore, there is valuable work ongoing to make the ordered arrangement of single-level building blocks into "one-piece" superstructure networks with tunable geometries and functional compositions. In this review, we first discuss the general strategies and underlying mechanisms for the fabrication of versatile carbon superstructures, such as flowers, urchins, and nanoarrays. The current design strategies are summarized and categorized into (i) the hydrothermal approach, (ii) the templating method, (iii) nanoemulsion assembly, (iv) spatially confined assembly, (v) modular self-assembly, and (vi) direct ink writing. Furthermore, we highlight the implementation performances of carbon superstructures as electrode materials for energy-storage devices, giving insights into the structure–property relationship in the family of nanomaterials. Ultimately, the challenges and outlooks of carbon superstructures in terms of design and uses are outlined to guide the future development of energy-related communities.

Anniversary statement

As an important forum of the materials chemistry community, the *Journal of Materials Chemistry A* covers high-quality research reports, involving the new synthesis, properties, understanding, and applications of materials related to energy and sustainable fields. For a long time, our research team has been committed to designing nanostructured carbon materials to drive energy technologies and has published a series of achievements in this journal. These studies have attracted a wide range of interest from a broad audience, with five of the articles selected in themed collections of the most popular articles, hot papers, or lunar new year collections. On the landmark occasion of the Journal of Materials Chemistry A's 10th anniversary, we dedicate this review article on carbon superstructures for energy storage as part of the anniversary celebrations. As one of the most abundant elements in nature, carbon plays a very important role in materials chemistry. Benefiting from structural tunability, chemical stability, and good conductivity, carbon materials have widely been used as efficient electrodes in an extensive spectrum of energy-storage technologies. Significantly, three-dimensional carbon superstructures with tailor-made morphologies and functionalities have attractive prospects as a new research direction to accelerate the development of carbon for advanced energy-storage applications.

1. Introduction

The rapidly increasing depletion of fossil fuels and the global environmental crisis call for the urgent development of sustainable and efficient energy-storage devices, such as zinc-ion hybrid capacitors, supercapacitors, and batteries.[1–5] The successful implementation of these electrochemical energy devices largely relies on the engineering of electroactive electrode materials, which store energy through different faradaic/non-faradaic charge-storage mechanisms.[6–8] Profiting from resource abundance, environmental benignity, and wide tunability in geometrical structure and surface chemistry, carbon-based materials are extensively studied as an important category of electrode materials for use in energy systems.[9–11] To date, a number of design strategies have been reported to upgrade the energy-storage metrics of carbon, entailing geometry regulation, pore-structure construction, and heteroatom introduction.[12–14] Despite some exciting achievements, the popularized carbon materials (*e.g.*, activated carbons, biomass-derived carbons, and graphite) still encounter the dilemmas of insufficient capacitive activity, limited high-rate survivability, and/or cycle stability resulting from the sluggish electrochemical kinetics and degenerated skeleton robustness.[15–18] One promising way out of the dilemma is to develop novel carbon materials with well-orchestrated structures and functions for comprehensively revolutionizing the energy storage of electrochemical devices.

In general, nanostructured carbon materials can be categorized into four categories according to their dimension numbers at the nanoscope scale: zero-dimensional (0D), one-

[a]Shanghai Key Lab of Chemical Assessment and Sustainability, School of Chemical Science and Engineering, Tongji University, Shanghai 200092, P. R. China. E-mail: ganlh@tongji.edu.cn; liumx@tongji.edu.cn

[b]College of Chemical Engineering, Zhejiang University of Technology, Hangzhou 310014, P. R. China

dimensional (1D), two-dimensional (2D), and three-dimensional (3D) materials.[19] Quantum nanodots and nanoparticles are often regarded as 0D nanomaterials,[20] while 1D materials generally include nanorods, nanotubes, nanofibers, and nanowires.[21] For 2D nanomaterials, nanosheets and nanomembranes are the typical series materials.[22–24] Graphene aerogels, honeycomb structures, and activated carbon are extensively investigated and used as 3D materials in appropriate fields and have obtained great successes.[25–27] Also, 3D carbon frameworks with hierarchical porous structures and functional compositions have attracted increasing attention in energy applications since they can prevent structure stacking to shorten the ion-diffusion distances and provide abundant ion-accessible active sites to support high electrochemical activity and durability.[11,28–30]

In particular, 3D carbon superstructures, constituted from the self-assembly or epitaxial growth of single-level building blocks, can deliver ingenious multiscale hierarchies and desirable functional attributes, and thus represent an appealing prospect for energy applications.[31–34] The isolated single-level segments (*e.g.*, nanosheets, nanorods, and nanoparticles) often suffer from structural instability and an electronic transport barrier due to the uncontrolled agglomeration of their nanosized configurations.[35] Making the well-organized arrangement of simple building blocks into integrative networks of superstructures can inherit the profitable properties of individual module elements, while also obtaining extra synergic benefits, including continuous charge-transport pathways, more exposed surface-active motifs, and robust frameworks with superior mechanical strength (Fig. 1).[36–40] However, it is exceedingly challenging to spark the spatially spontaneous nanoarchitecturing of low-dimensional building blocks to construct integrative superstructures, especially by facile and highly efficient routes. To date, significant advances have been made in fabricating carbon superstructures with tailor-made

Ziyang Song is a postdoctoral fellow in Prof. Mingxian Liu's group at Tongji University. He received his PhD degree from the School of Chemical Science and Engineering, Tongji University, Shanghai (2021). His research interests are focused on the structural design of redox-active organic materials and porous carbons for energy applications, including zinc–organic batteries, zinc-ion hybrid capacitors, and carbon-based supercapacitors.

Ling Miao received her BS. degree and PhD degree from the School of Chemical Science and Engineering, Tongji University, Shanghai (2018). She started her postdoctoral research at Tongji University (2018–2022). After that, she joined the School of Chemical Science and Engineering at Tongji University as an assistant professor in 2022. Her research interests are focused on the design and tailored synthesis of ionic liquid-derived electrode materials in the fields of supercapacitors, zinc-based energy-storage systems, and their hybrids.

Yaokang Lv received his first PhD degree from the Department of Chemistry, Tongji University (2014); his second PhD degree was awarded by the Institut de Chimie, Université de Strasbourg (2021). He started his postdoctoral research at Tsinghua University (2014–2017) and joined the College of Chemical Engineering at Zhejiang University of Technology as a teacher. His current research interests include the synthesis and recycling of materials for energy storage and/or electrochromic devices, and packaging, as well as pollutants treatment.

Lihua Gan received his PhD degree in Materials Physics and Chemistry from Tongji University, and became a professor at the School of Chemical Science and Engineering of Tongji University (2005). His research interests include the design and application of nanomaterials, including porous metal oxides, various carbonaceous materials, and carbon-based materials. These nanomaterials are used in supercapacitors, lithium-ion batteries and as adsorbents for pollutants treatment.

Mingxian Liu received his PhD degree in physical chemistry from Tongji University (2009). He started his postdoctoral research at the East China University of Science and Technology (2009–2011). After that, he joined the School of Chemical Science and Engineering at Tongji University, and became a professor in 2016. His current research interests are focused on the structural design of electrode materials for electrochemical energy storage, including carbon-based supercapacitors, zinc-ion hybrid supercapacitors, and zinc-ion batteries.

morphologies and potentially favorable properties for energy storage, but comprehensive overviews of the diverse carbon superstructures remain lacking.

In this review, we strive to give an overview of the design, synthesis, and application of versatile carbon superstructures with well-defined micro-/nanoscale configurations, such as flowers, urchins, tube-sheet hierarchies, and nanoarrays. The general synthetic methods and formation mechanisms for carbon superstructures are summarized and classified, including the hydrothermal method, templating approach, nanoemulsion assembly, spatially confined assembly, modular self-assembly, and direct ink writing. The detailed discussion of each type is illustrated with representative examples. Then, we demonstrate the potential applications of the carbon superstructures for energy storage. Lastly, the future development directions, opportunities, and challenges associated with carbon superstructures in the energy-related realms are discussed.

2. Design strategies and underlying mechanisms

2.1 Hydrothermal approach

The hydrothermal strategy refers to the solvothermal chemical reaction performed under high temperature and pressure in a sealed pressure vessel, which is a forceful technology for customizing various carbon nanomaterials, especially spherical carbon superstructures.[41,42] Materials in nature follow the laws of natural selection and tend to form spherical configurations with minimized energy.[43,44] Regular spherical superstructures featuring a close-packed nature and high-density accessible active sites can facilitate ion diffusion over short lengths,[45–47] and are particularly useful for energy storage. Thus, the elaborate engineering of spherical carbon superstructures is of great significance from both a fundamental and technological viewpoint.

As an alternative strategy, solvothermal methods can empower the straightforward and scalable construction of new types of carbon superstructures.[48,49] Recently, Xu's group reported self-ordered chestnut-shell-like carbon superstructures constructed from 1D anisotropic metal–organic framework (MOF) nanorods of about 10 μm through the hydrothermal transformation of MOF nanoparticles (Fig. 2a), triggered by the coordination reaction of zinc acetate dihydrate and 2,5-dihydroxyterephthalic acid using urea as a modulator.[50] Interestingly, the nanorods grew orderly on hollow shells to yield nanorod-constituted MOF superstructures, which could be applied as organic precursors for fabricating spherical carbon superstructures with well-preserved geometries after pyrolysis (Fig. 2b and c). Further, spherical superstructures with a controlled size of 1.4–5.2 μm constructed from small nanosphere building blocks (120–360 nm) were fabricated by the hydrothermal carbonization of glucose with the help of poly(4-styrenesulfonic acid-co-maleic acid) (PSSMA) sodium salt and hydrochloric acid (Fig. 2d).[51] High temperature and pressure solvothermal conditions facilitated the formation of glucose nanospheres, and then the structure-directing agent PSSMA was adsorbed on the nanosphere surfaces to restrain their growth speed and offer intermolecular electrostatic repulsive force. Meanwhile, the hydrochloric acid promoted the hydrothermal carbonization to yield nanoparticle nuclear structures in the incipient state, and subsequently, the nanospheres spread on them to generate large-sized superstructural spheres (Fig. 2e and f).

Furthermore, the hydrothermal method has been utilized to synthesize a series of flower-shaped carbon superstructures.[32,40,52] For instance, Zhang's group designed 3D hierarchical carbon superstructures consisting of ultrathin nanosheets *via* a hydrothermal intercalation growth strategy (Fig. 2g).[53] This involved the construction of flower-shaped sandwich-type carbon/Zn_2SiO_4 hybrids based on the solvothermal reaction between $Zn(C_6H_{11}O_7)_2$ and SiO_2. Subsequent removal of the Zn_2SiO_4 layers yielded graphene-like

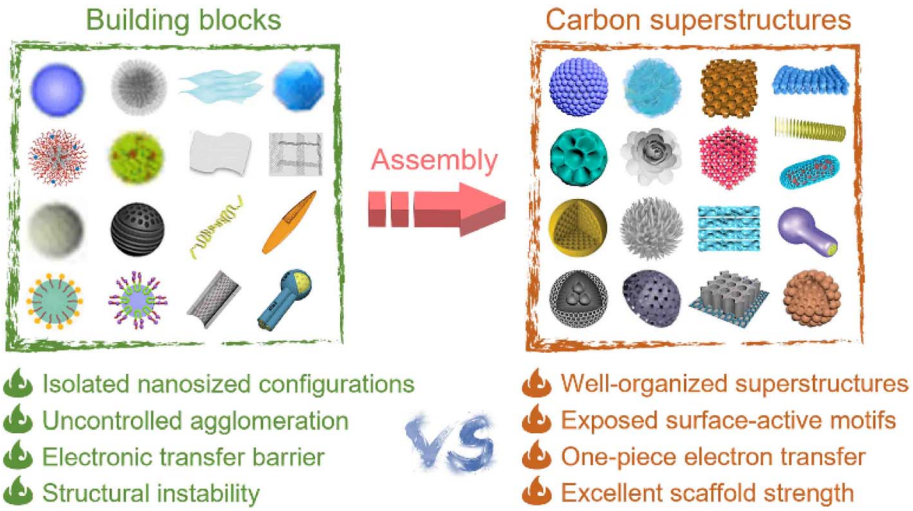

Fig. 1 Features of carbon superstructures compared with their building blocks.

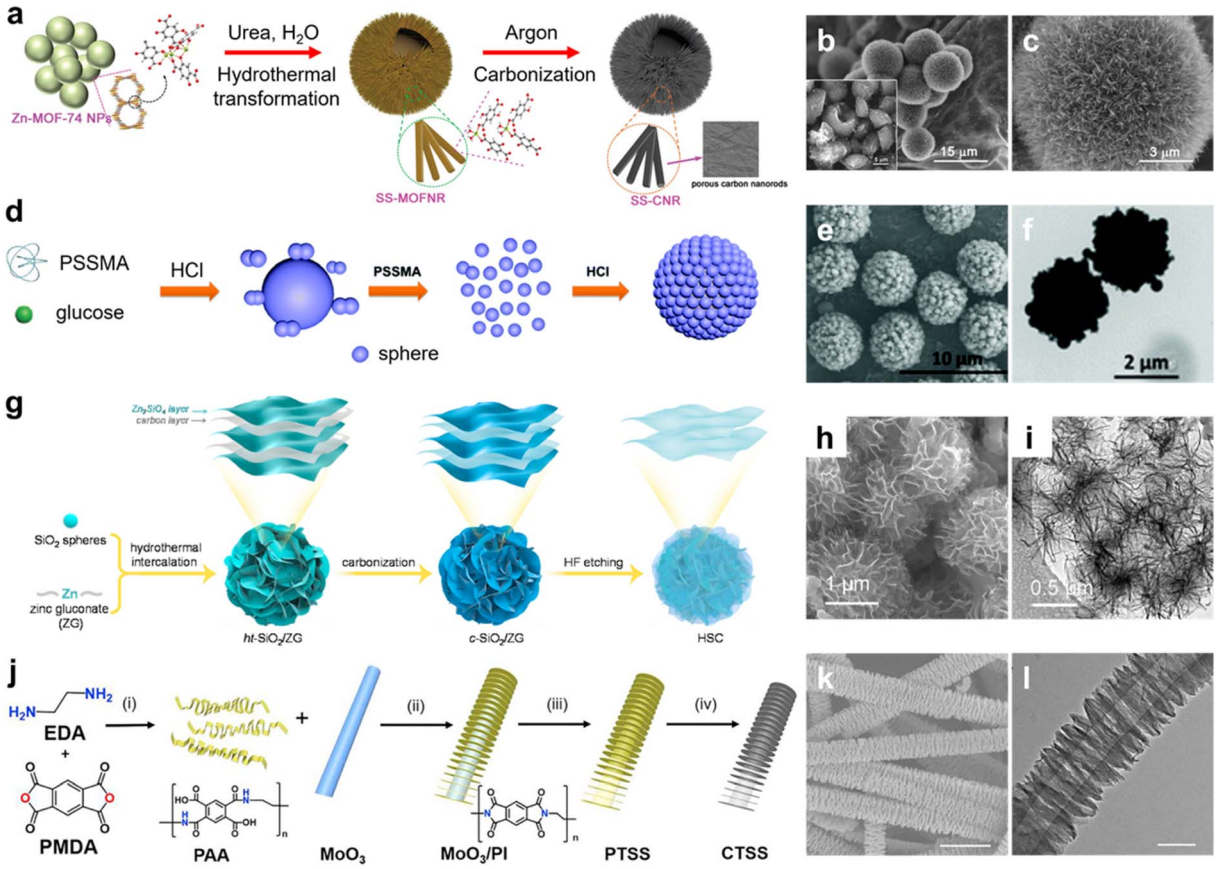

Fig. 2 (a) Fabrication of nanorod-constituted carbon superstructures. (b) Scanning electron microscopy (SEM) and (c) transmission electron microscopy (TEM) images of carbon superstructures. Reproduced with permission.[50] Copyright 2019, Wiley-VCH. (d) Fabrication scheme of carbon nanospheres. (e and f) Structural images of colloidal carbonaceous spherical superstructures. Reproduced with permission.[51] Copyright 2018, The Royal Society of Chemistry. (g) Synthesis process of flower-shaped carbon superstructures. (h) SEM image and (i) TEM image of multiscale hollow carbon hydrangeas. Reproduced with permission.[53] Copyright 2021, Elsevier. (j) Schematic synthetic procedure toward ordered carbon tube-sheet superstructures and (k and l) corresponding structure images. Reproduced with permission.[56] Copyright 2019, Elsevier.

interconnected self-supported ultrathin carbon nanosheets (<1 nm in thickness), affording robust hierarchical superstructured carbon networks (Fig. 2h and i). Profiting from amorphous feature with rich structural defects, the carbon superstructures delivered a large pore volume and surface area for efficient charge storage. Additionally, the as-prepared superstructures were able to be spread on the surfaces of different SiO_2 substrates to craft carbon materials with variant superstructural geometries. Recently, the spheroidizing growth of moldy flour with the aid of a cyanurate-melamine structure-directing agent was reported to construct functional carbon flowers.[54] Similarly, homogeneous hydrangea-like submicron hollow carbon spheres were fabricated by the direct hydrothermal treatment of glucose with fibrous silica spheres as a shape guide, followed by pyrolysis and template etching.[55] The as-prepared carbon hydrangeas consisting of petal-like partially graphitized nanosheets exposed a refined surface texture with enormous tunnels and furrows, making them attractive materials for energy applications.

More interestingly, based on a hydrothermal-assisted self-assembly strategy, Wu's group created a multilevel carbon tube-sheet superstructure with vertically periodic nanosheet arrays, applying polyimide as the carbon precursor and MoO_3 nanorod as the template (Fig. 2j).[56] By changing the reaction circumstances, the geometries of polyimide nanosheet arrays could be tuned in size (340–750 nm) and periodicity (40–75 nm) (Fig. 2k and l), allowing the achievement of carbon superstructures with fine-tunable architectures. Considering the diverse polymerization chemistry with designable precursor structures, the hydrothermal protocol is anticipated could extend the family of carbon superstructures with a variety of functions and applications.

2.2 Templating method

The templating method is a well-developed strategy to synthesize carbons with required configurations.[57–59] During high-temperature carbonization, carbon materials must follow the principle of the minimum surface energy by decreasing their surface area to form a stable architecture. Unfortunately, efficient energy-storage devices require carbon electrodes with large surface areas. The addition of templates can surmount

this problem well. During the reaction process, carbon precursors are wrapped on the template surface to generate composites, which effectively reduce the energy of entire materials. Meanwhile, the templates advantageously hold the carbon structures. After removing the template and carbonization, the carbons retain the space occupied by the templates to form opposite structures.[60] Thus, the shape of the template is a crucial factor in the synthesis process, helping determine the shape of the ultimate carbon structures. According to the different types of templates, the templating strategies can be divided into hard, soft, and hybrid templating methods.[61]

Over the past several decades, the hard-templating strategy has been widely applied for control over carbon textures.[35,62,63] The applied solid templates (silica, polystyrene, ferric oxide, *etc.*) allow inversely replicating the intrinsic architectures into the final carbon materials.[27,30,64–68] For instance, Yu's group fabricated high uniformity 3D ordered macroporous carbons through the *in situ* growth of ZIF-8 precursors between the clearances existing in the neighboring polystyrene solid nanoparticles, followed by the removal of the polystyrene template and heat treatment in an argon atmosphere (Fig. 3a).[69] Such bicontinuous porous frameworks showed interconnected macropores (~170 nm, Fig. 3b and c) and a large surface area (820 $m^2 g^{-1}$), which boosted the mass diffusion properties and led to more active sites exposed and improved electronic conductivity, giving them superior electrochemical activity and cyclability for K-ion storage. Another similar example was the direct pyrolysis of polydopamine (PDA)/polystyrene (PS) composited precursors to fabricate honeycomb-like carbons.[70] Such open macroporous structures could stimulate the permeation of electrolyte ions inside the electrodes even at large current rates, thus endowing significant rate-performance metrics. Further, Yang and coworkers developed hierarchical sphere-in-tube porous superstructures *via* confining SiO_2 particles within anodic aluminum oxide channels and by subsequently filling polypyrrole precursor solution, followed by pyrolysis and acid etching.[71] The as-designed carbon nanoarchitectures harvested better capacitive characteristics than those of pure nanotubes/hollow spheres.

With regard to the soft templating method, block copolymers are commercially available as efficient templates due to their rich self-assembly phase diagrams.[72–74] Tunable hollow ordered mesopore structures can be directly formed in carbon materials *via* self-assembly between micelles of amphiphilic block copolymers and organic precursors. The most common ones include PS–P4VP/PEO, PPO–PEO–PPO, and PEO–PPO–PEO

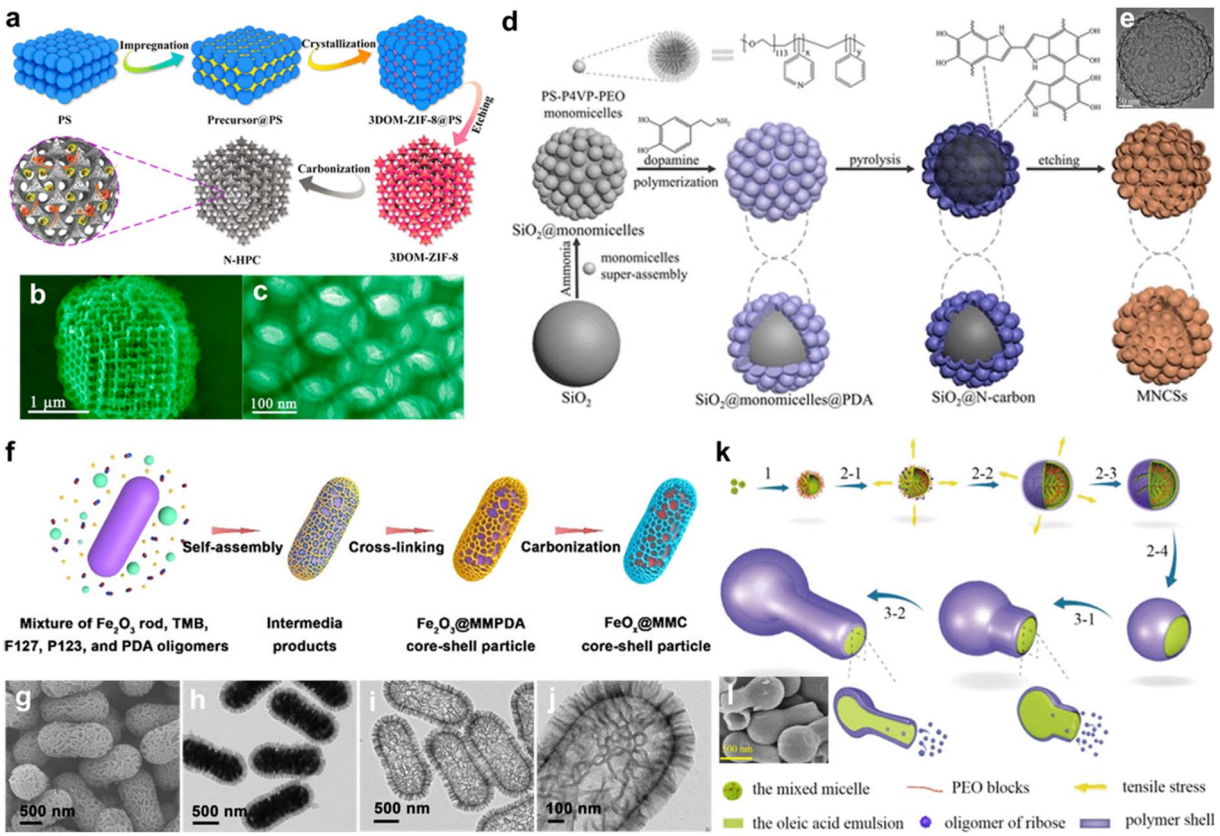

Fig. 3 (a) Fabrication procedure of 3D interconnected hierarchical porous carbons and their (b and c) structural images. Reproduced with permission.[69] Copyright 2019, American Chemical Society. (d) Fabrication scheme of 3D hollow hierarchical carbon superstructures and (e) their TEM image. Reproduced with permission.[86] Copyright 2022, American Chemical Society. (f) Schematic illustration of the complex double-layer carbon nanoshells, SEM and TEM images of (g and h) FeO_x@Fe carbon-based composite particles and (i and j) macro-/mesoporous carbon nanoshells. Reproduced with permission.[67] Copyright 2020, Wiley-VCH. (k) Growth mechanism of asymmetric hollow carbon flasks and corresponding (l) SEM image. Reproduced with permission.[87] Copyright 2017, American Chemical Society.

(PPO: polyethylene oxide; PEO: polypropylene oxide; P4VP: poly(4-vinyl pyridine)), which can be eliminated during the pyrolysis process.[75–78] To achieve large mesopores in carbon nanospheres, the PS-*b*-PEO template was applied during the growth process of PDA precursor. Subsequent carbonization removed the sacrificial PS-*b*-PEO micelles and led to large mesopores (16 nm) in the final spherical carbons (300 nm).[79] Besides the regular mesoporous nanospheres, soft-templating strategies can be further expanded to build novel morphologies and pore structures, such as walnut-shaped particles,[80] asymmetric bowl-like mesoporous particles,[81] triple-shelled hollow spheres,[82] dendritic mesoporous nanospheres,[83] and other complicated nanoarchitectures[84] that synergize the accessible active interfaces/interior spaces into a single system. These approaches provide good opportunities to tune the soft template-mediated assembly process for producing various carbon materials with controllable superstructures.

Complex and ordered architectures generally are difficult to realize with a single hard or soft templating method. Combining hard–soft templating approaches though can engender an exciting avenue to create carbon materials with exquisite superstructures.[85] Zhao's group synthesized brand-new N-doped mesoporous superstructural carbon spheres through a monomicelle interface confined assembly approach (Fig. 3d).[86] Such supraparticles were composed of a large central cavity with a diameter of 300 nm, an ultrathin monolayer of spherical mesopores (~22 nm), and small pores (4.0–4.5 nm) on the interior surfaces of spherical mesopores (Fig. 3e), allowing totally interconnected mesoporous superstructures with good underwater aerophilicity and a large surface area (685 $m^2 g^{-1}$). In addition, the structure parameters of the supraparticles, such as mesopore number, size, and shell thickness could be precisely regulated. Such a strategy enables the accurate fabrication of mesoporous carbon superstructures with variable architectures, including 2D nanosheets, 3D nanospheres, and nanovesicles. Guan's group proposed a general heterogeneous nucleation strategy for the precise tailored coating of hierarchical macro-/mesoporous carbonous nanoshells (Fig. 3f) with radial ultra-large channels (10–200 nm) on colloidal Fe_2O_3 rods to form core–shell nanostructures (Fig. 3g–j).[67] Modulating the self-assembly behavior of irregular bicontinuous structural units (P123/F27-PDA nanocomposites) could finely tune the macro-/mesostructured interparticle space on different core materials, thus allowing interfacial assembly in a loose packing mode to form various shell nanomaterials with controllable geometries. This dual template method gives a novel toolbox for the creation of carbons with exquisite core–shell configurations and ultra-large open channels.

Dual soft-templating approaches have been adopted and applied in the design of multi-model carbon superstructures for use in energy storage. For instance, there was interesting asymmetric hollow open carbon nanoflasks were prepared through a dynamic growth mechanism triggered by the synergistic interactions between ribose (carbon source) and dual soft-templates (sodium oleate and P123 copolymer) (Fig. 3k and l).[87] Specifically, during the hydrothermal process, the ribose precursors provided an acid condition for sodium oleate, in which the oleic acid nanoemulsion was initially formed and acted as both a benign solvent and template for the amphiphilic derivatives of the precursor. Meanwhile, P123 promoted the homogenous dispersion of the nanoemulsions and induced the cracking of carbonaceous shells to offer openings. These interactions triggered the generation of hollow asymmetric carbon flasks. This work enables access to novel inspirational methodologies for exploring anisotropic carbon nanomaterials with high structural complexity.

2.3 Nanoemulsion assembly

A typical liquid–liquid interface synthetic example is microemulsion, which involves the mixing of oil and water in the presence of surfactants. It has been extensively used as a confined reaction medium for designing mesoporous carbons, but normally triggers nanoscale spherical ones, such as bowl-like or walnut-shaped.[88] Recently, Zhao's group reported a versatile nanoemulsion assembly strategy to construct uniform nanoscaled carbon spheres with accessible mesopores (5–37 nm) *via* applying a dopamine (DA) precursor, F127 template, 1,3,5-trimethylbenzene (TMB), and ammonia catalyst in an ethanol–water mixed solvent (Fig. 4a).[89] The representative dendritic carbon nanospheres (Fig. 4b) displayed a small particle size (128 nm), large pore size (37 nm), plentiful N content (6.8 wt%), and accessible surface area (635 $m^2 g^{-1}$), which exhibited their great prospect for advanced energy storage. Mechanistic studies revealed that the amount of organic TMB molecules affected the F127/DA interface interactions and afforded a key role in the evolution of pores. Well-defined DA/TMB/F127 nanoemulsions could be facilely formed in mixed ethanol/water solvents, which could then guide the assembly of PDA into homogeneous polymeric nanospheres and mesoporous carbon derivatives with distinctive architectures, such as smooth, golf ball, multichambered, and dendritic nanospheres.

This nanoemulsion strategy gives an appealing insight into the use of interfacial assembly for the design of carbon superstructures, which could be easily expanded to fabricate multi-model superstructures with desirable morphologies.[90,91] For example, Li and coworkers employed the nanoemulsion self-assembly method to prepare multilevel carbon frameworks with high structural complexity (Fig. 4c).[57] In this case, DA-polymerized PDA interacted with spherical TMB/F127 micelle cores *via* noncovalent self-assembly and covalent bonds. Driven by shear force, the monodisperse spherical micelles coated with PDA were further assembled into a vertical mesopore array on the hydrophilic surface of the graphene oxide nanosheets. Similar mesopores could be obtained within the carbon foams after freeze drying to obtain a robust precursor architecture with subsequent carbonization for pore engineering. More recently, Zhao's group intelligently synthesized radially gradient-pore core–shell mesoporous carbon spheres through a programmable shear-induced dynamic assembly route (Fig. 4d).[92] The growth kinetics of DA could be guided through establishing an on-demand stirring model (350–500 rpm) to alter the shear force. This led to the programmed assembly of 3D multimodal

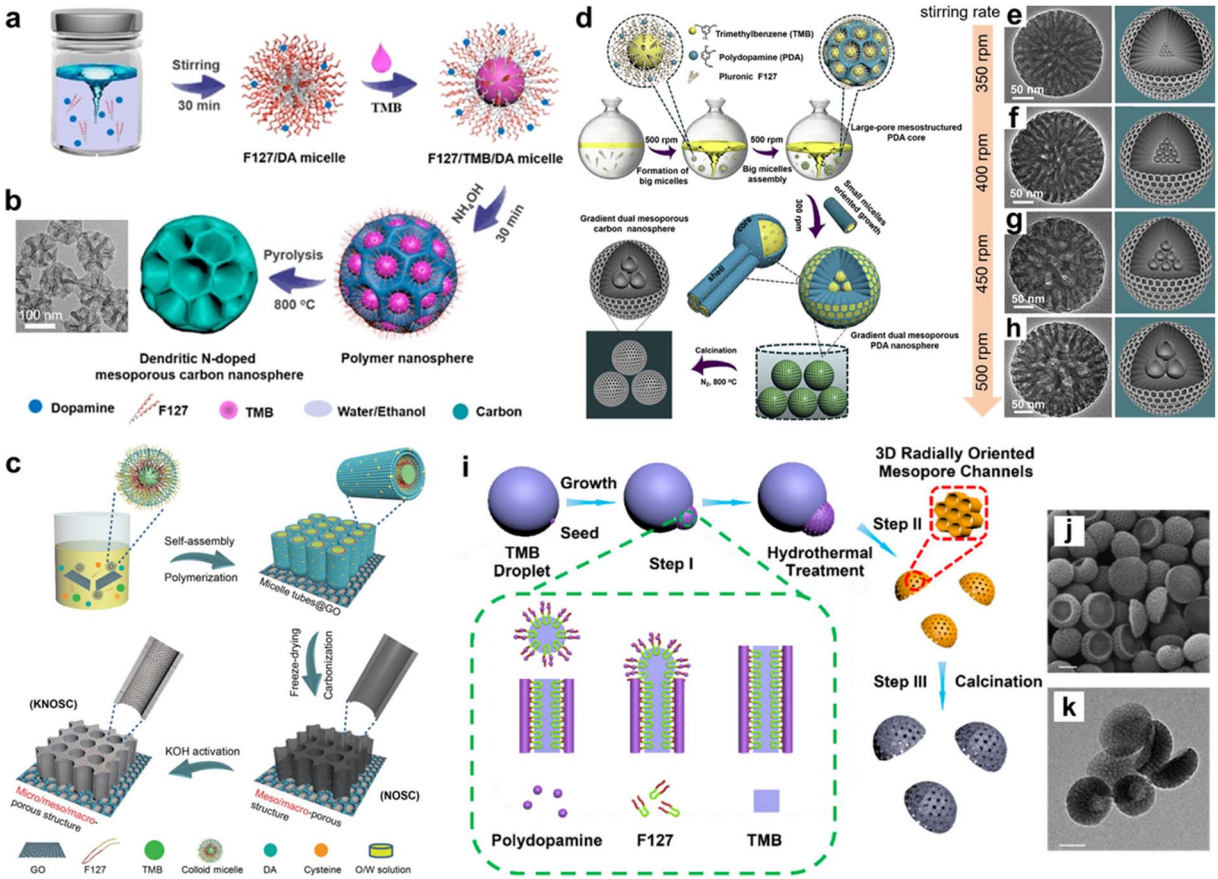

Fig. 4 (a) Schematic illustration of the construction process for dendritic mesoporous carbon nanospheres and (b) corresponding TEM images. Reproduced with permission.[89] Copyright 2019, American Chemical Society. (c) Fabrication of carbon foams. Reproduced with permission.[57] Copyright 2019, Wiley-VCH. (d) Schematic assembly of gradient-pore carbon spheres and (e–h) corresponding structural models. Reproduced with permission.[92] Copyright 2021, Elsevier. (i) Fabrication scheme of spiral multi-shelled carbon nanospheres and corresponding (j) SEM image and (k) TEM image. Reproduced with permission.[88] Copyright 2016, American Chemical Society.

open superstructures with adjustable surface areas (414–686 m^2 g^{-1}), particle sizes (200–230 nm), and mesostructures (7.0–24.0 nm) (Fig. 4e–h). Similarly, Lou's group synthesized high-surface-area bowl-like carbon particles with radially oriented mesopores (~8 nm) by a facile emulsion–driven interface anisotropic assembly method (Fig. 4i–k).[88]

Another interesting superstructure design is multimodal supraparticles with unique spiral architecture.[93] Zhao and coworkers synthesized mesoporous multi-shelled carbon spheres with a chiral architecture based on a layered micelle spiral self-assembly strategy.[94] Different from conventional chiral templating approaches, this synthesis introduced shearing flow to propel the intelligent spiral growth of the lamellar P123/TMB/DA micelle system into multi-shelled nanospheres. The mechanical interactions between the layer-to-layer forces and intralayer bending energy provided the cornerstone for constructing helical architectures with amphiphilic triblock copolymers. Taking the regulation of the amphipathicity of surfactants as the clue, and the packing parameters of surfactant micelles as the theoretical basis, diverse mesoscopic superstructures were fabricated by applying various templates, entailing single-cavity smooth, flower-shaped, radially oriented, and spiral multi-shelled spherical superstructures. The unprecedented spiral superstructures integrating a large surface area (530 m^2 g^{-1}), abundant mesopores (2.5 nm), and N heteroatoms (6.2 wt%) exhibited great application prospects toward energy storage. This powerful nanoemulsion strategy provides new inspiration for the future superstructure engineering of carbons with diverse morphologies and functionalities.

2.4 Spatially confined assembly

Carbon microcapsules with porous shells and large interior cavities are desirable hosts for guest species, but maximizing the in-cavity volume is still challenging for researchers.[95–97] In comparison to the above methodologies, the creation of mesoporous spherical structures in a confined space is conceptually straightforward, and can be executed by controlling the polymerization parameters. Taking a recent classical study as an example, Sun and coworkers developed a spatially confined self-assembly approach to prepare microspheres with a variable symmetry of mesostructures and discrete spherical architectures by using phenolic resol carbon source and silica/F127 dual templates (Fig. 5a).[98] The monolithic opal architectures of PS

microspheres were initially synthesized and duplicated with an ethanolic silicate solution, resulting in the formation of 3D ordered macroporous monolith templates. Then, injecting a mixed solution of F127 and phenolic resol precursor into the ordered macroporous voids of the 3D monolith template facilitated the confined self-assembly process. After solution evaporation, pyrolysis, and template removal, orderly aligned mesoporous carbon microspheres could be harvested (Fig. 5b and c), which possessed large mesopores (7–10.3 nm), variable surface areas (500–1100 $m^2 g^{-1}$), and pore volumes (0.6–2.0 $cm^3 g^{-1}$).

Besides, the carbon microsphere size could be facilely adjusted by applying different-sized templates.

Interestingly, this method has been refined to fabricate other types of multilevel-structured carbon spheres. Lu and coworkers synthesized grid-like multicavity carbon microspheres by a surface free-energy-induced assembly method (Fig. 5d), based on the spontaneous growth and assembly of resol precursors within the small-sized nanoemulsion-confined space.[99] In addition, the size and number of microsphere cavities could be finely tuned by altering the size of the nanoemulsion and concentration of the polymer, and confined pyrolysis could further enlarge the cavity size. This surfactant-directed space-confined polymerization strategy could be extended to create exquisite multichamber carbon microspheres by employing 2,6-diaminopyridine (DAP) and formaldehyde precursors, sodium dodecylbenzene sulfonate (SDBS), and F127 as dual surfactants (Fig. 5e).[100] The synthesis of multichamber carbon microspheres was accomplished in three steps. The first step involved the incubation of cytoskeleton-like DAP-formaldehyde (DAP-F) spheres, wherein F127 acted as the steric stabilizer and SDBS formed vesicles with DAP-F. Subsequently, acetic acid catalyst promoted the further cross-linking of the DAP-F prepolymer. The confinement of polymerization in the microspheres led to the space separation of large chambers and the generation of several tiny multi-chambers (Fig. 5f–i). The third step was to build high-surface-area (up to 1797 $m^2 g^{-1}$) and high-N-content (4.58 wt%) microspheres with multichamber cores and microporous shells after carbonization/activation in a N_2/CO_2 atmosphere (Fig. 5j–m).

2.5 Modular self-assembly

Organizing low-dimensional modules into integrative superstructures delivers attracting prospects due to their synergistically structural and functional natures.[101–103] Current achievements are mostly related to modular self-assembly and center on inorganic colloidal particles (Fe_3O_4, SiO_2, Ag, *etc.*) owing to their good thermodynamic stability.[104–109] Nevertheless, in most scenarios, inorganic particle-constituted superstructures are generally superlattice configurations, originating from the conventional one-by-one close packing of the building blocks, which makes it difficult to form hierarchical superstructures *via* super-assembly on the interface.[110,111] The modular self-assembly entails the primary construction of single-level building blocks (such as nanosheets, nanorods, and nanoparticles) by pairing judicious precursors with rational processing techniques, and by further manipulating their spontaneously spatial well-organized arrangement into "one-piece" superstructure networks with a multiscale hierarchy and desirable functional attributes. Compared with the templating methodology that harnesses the inverse replication of intrinsic structures of the applied soft/hard templates to form structure-specific carbons, the modular self-assembly strategy does not involve the application/removal of templates, or complicated and time-consuming procedures, thereby enabling the facile and versatile customized nanoarchitecturing of ingenious carbon superstructures. Therefore, it is necessary to develop organic modules and govern their self-assembly to create novel carbon superstructures.

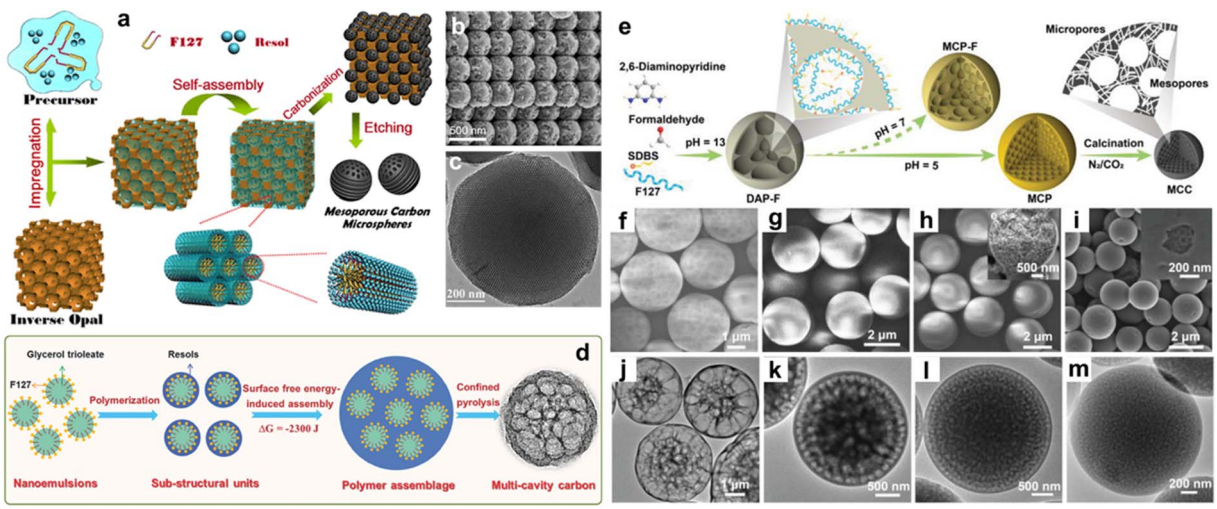

Fig. 5 (a) Fabrication of ordered macroporous carbon microspheres. (b) SEM image and (c) TEM image of the uniform carbon microspheres. Reproduced with permission.[98] Copyright 2013, American Chemical Society. (d) Preparation of multicavity carbon spheres. Reproduced with permission.[99] Copyright 2017, Wiley-VCH. (e) Spatially confined assembly of multichamber microspheres and corresponding (f–i) SEM and (j–m) TEM images. Reproduced with permission.[100] Copyright 2019, Wiley-VCH.

Recently, some endeavors harnessing organic subunits (*e.g.*, nanorods, nanosheets, and nanoparticles) have been made to harvest superstructural carbon materials with ultrahigh stability.[112] For example, our group developed a facile self-assembly route to construct well-defined carbon superstructures consisting of nanoparticle-embedded plates (Fig. 6a).[38] Mechanism investigations unraveled that 2,4,6-trichloro-1,3,5-triazine and 2,6-diaminoanthraquinone could interact to form a rigid organic skeleton with a hexameric "protic salt"-like structure bridged by $-NH_2^+Cl^-$– "rivets" (Fig. 6b), which offered the cornerstone for the self-assembly of the polymeric framework of superstructures *via* H-bonding and π–π stacking (Fig. 6c). The polymer superstructures could be expediently converted into hierarchical carbon superstructures with a well-inherited morphology through synchronous carbonization and activation (Fig. 6d). Featuring nanoparticle-interconnected robust skeletons, the carbon superstructures showed abundant electroactive motifs and fast electrochemistry kinetics for achieving excellent energy storage.

Further, Zhao's group synthesized all-in-one covalent organic framework (COF)-based microflowers with interconnected hollow petals through a one-step self-template strategy (Fig. 6e).[113] Morphology evolution at different reaction stages untangled that the hollow micro-flower superstructures originated from the collaborative growth mechanism of nanoparticle self-assembly, inside-out Ostwald ripening, and epitaxial growth. The advantages of hollow superstructure and the inherent porosity of the superstructures were highlighted by the all-round performance improvements in supercapacitors (Fig. 6f and g). More recently, our group reported a Lewis pair interaction-guided self-assembly route to access well-organized carbon superstructures built of nanotentacle building blocks, based on the acid–base interaction between ferric chloride (Lewis acid) and *p*-phenylenedimethanol (Lewis base) through H-bonding and π–π stacking (Fig. 6h and i).[114] The proposed design strategy gives new opportunities for customizing delicate carbon superstructures.

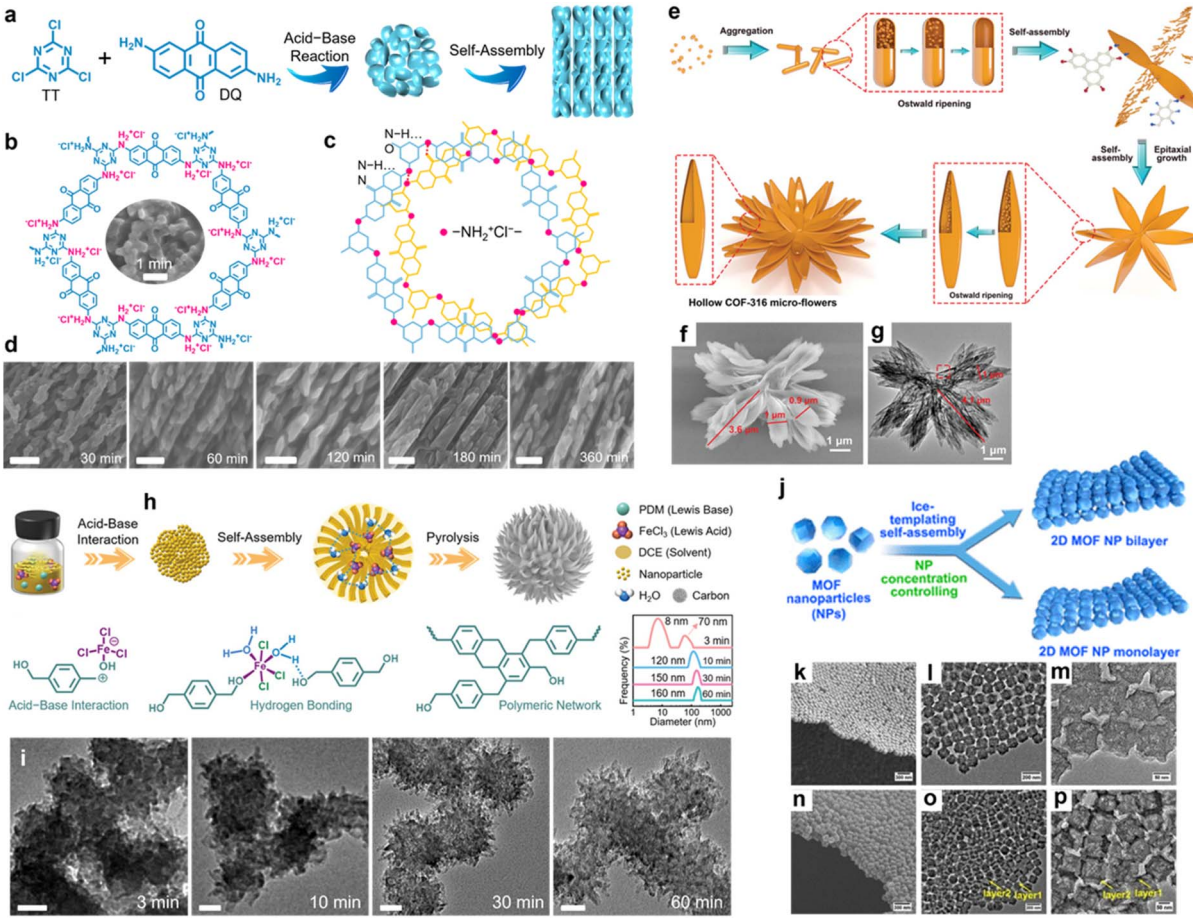

Fig. 6 (a) Construction scheme of nanoparticle-constituted carbon superstructures. (b) "Protic salt"-like conjugated polymer framework. (c) H-bond interactions between carbonyl groups and $-NH_2^+Cl^-$– linkers. (d) SEM images of carbon superstructures. Scale bar: 200 nm. Reproduced with permission.[38] Copyright 2021, Wiley-VCH. (e) Formation mechanism of hollow COF microflowers and corresponding (f) SEM image and (g) TEM image. Reproduced with permission.[113] Copyright 2021, Wiley-VCH. (h) Schematic representation of the synthesis of carbon superstructures by Lewis pair interaction and H-bond effect. (i) TEM images of the polymers collected at various polymerization times. Scale bar: 50 nm. Reproduced with permission.[114] Copyright 2022, Wiley-VCH. (j) Formation process of 2D carbon mono-/bilayers of interconnected hollow carbon superstructures. SEM and TEM images of (k–m) monolayer superstructures and (n–p) bilayer superstructures. Reproduced with permission.[33] Copyright 2022, American Chemical Society.

Ice-templating, also known as freeze-casting, is a facile and diverse technology that has been widely used to create hierarchically well-aligned porous materials.[115–117] Encouragingly, ice-templating-driven self-assembly delivers great potential to fabricate superstructural carbon materials. As the first demonstration, Yamauchi and coworkers synthesized nanoparticle-constituted 2D layered MOF superstructures through an ice-templating self-assembly approach without any surfactants or external fields (Fig. 6j).[33] Regulating the concentration of precursor colloidal MOF nanoparticles realized monolayered (Fig. 6k–m) and bilayered superstructures (Fig. 6n–p). Adjacent polyhedral MOF nanoparticles were packed and arranged *via* the crystal facet to form quasi-ordered array superstructures. Triggered by the outward contraction of the MOF precursors during carbonization, the MOF superstructures were stable and could be easily converted into carbon products with a well-maintained morphology, hollow interiors, and high exposure of active sites. Such an achievement demonstrated that ice-templating is a powerful protocol for the construction of versatile carbon superstructures.

2.6 Direct ink writing

Conventional synthesis methods like all the aforementioned strategies have difficultly accurately formulating arbitrary carbon geometries with tailor-made features. If programmable geometries and serial interior channels could be created, the electrochemical reaction kinetics of carbon superstructures could be essentially boosted, which would benefit superior charge storage at high currents.[118,119] Therefore, alternative manufacturing techniques must be sought to realize this goal.

Direct ink writing, a type of extrusion-based 3D printing technology, is becoming a powerful tool for engineering superstructural carbon materials.[119] Direct ink writing adopts a computer-programmed translation stage, in which the ink deposition nozzle is moved to write a patterned structure through continuous filament writing.[120] The filaments extruded from the printing nozzle stack layer by layer, and finally build a pre-modeled 3D architecture. As the nozzle movement is digitally governed by the input computer program code, direct ink writing can arrange the carbon geometries into pre-designed patterns.[121] The most important component of direct ink writing is the ink materials. Inks extruded from printing nozzles should produce continuous and self-supporting filaments that resist collapse, spread, or sag.[122,123] To meet this demand, the ink materials must be fluids with shear-thinning rheological characteristics: the fluid viscosity should sharply reduce under shear force, and quickly recover when the force is removed.[120] Although most of the available writing inks are polymers and metals, some electrochemical active inks, such as graphene hydrogel and cellulose nanocrystal-based inks, have been successfully applied for energy storage.[124–126]

Over the past few years, freestanding graphene-based paper-like architectures have seen considerable progress in the exploration of advanced energy-storage systems owing to their high electrical conductivity (10^3–10^4 S m^{-1}) and large surface area (up to 2630 m^2 g^{-1}).[127,128] The 3D direct ink writing technique represents a great opportunity to construct large-area and low-cost graphene papers with a controlled thickness and dimension. In particular, graphene oxide (GO) has been a crucial 3D printing ink for the design of graphene-based materials. Recently, Wang and coworkers developed a new type of nanohybrid papers based on the well-controlled full inkjet printing synthesis of a freestanding graphene paper (GP)-supported 3D porous graphene hydrogel (GH)-polyaniline (PANI) nanocomposite (GH-PANI).[129] As shown in Fig. 7a, a 3D GH-loaded PANI ink was first prepared by ball milling and ultrasound treatment of GH-PANI nanomaterials in water. Meanwhile, the GO ink was printed on a commercial paper substrate by direct ink writing to form a GP. Then, the GH-PANI ink was overprinted on GP to form a freestanding GP-supported GH-PANI nanocomposite through π–π stacking. After hydroiodic acid reduction, the freestanding GH-PANI/GP was stripped from the commercial paper substrate.

High GO concentration-based inks generally are highly susceptible to multicomponent non-homogeneity, while the harsh post-treatment for additives removal may damage the physiochemical nature of the printed components.[130] To overcome these limitations, Fan's group proposed a generalized 3D printing methodology for designing graphene-based mixed-dimensional (2D + *n*D, where *n* is 0, 1, or 2) hybrid graphene aerogels with complicated superstructures (Fig. 7b).[131] They developed gel-like hybrid inks whose rheology could be regulated by urea. In this case, urea endowed a liquid-like response to the ink and improved the strength and elasticity of the printed gel by over an order of magnitude. Importantly, the shape-conformable printing of out-of-plane patterns on curved surfaces was also demonstrated, enabling mixed-dimensional hybrids with printability and geometry-versatile programmability. Highly coordinated networks within their structural framework contributed to successive electron- and ion-transport pathways and increased electrochemical performances. Such an improvement highlights the enormous application potentials of superstructural carbon aerogels for energy storage.

Although graphene and GO have been printed in earlier times, the customized assembly of graphite (hundreds of graphene layers) into diversified 3D superstructures *via* the direct ink writing method was not reported until the recent work of Ajayan *et al.*[132] The biggest challenge for printing hundreds of graphene layers is to maintain the continuity of the printing and to prevent particles from blocking during extrusion.[133] Ajayan and coworkers proposed a solution to surmount this limitation by formulating a nanoclay-modified graphite-based colloidal ink, which allowed the construction of complex architectures with adjustable geometries and directionalities by 3D printing at room temperature (Fig. 7c). The nanoclay could be easily adapted into the graphite layers, forming strong binding between the layers to make larger structures. Without further heat treatment, the direct ink writing of complex graphitic structures could make shape engineering and related applications of graphite at various length scales easier. The printed architectures showed

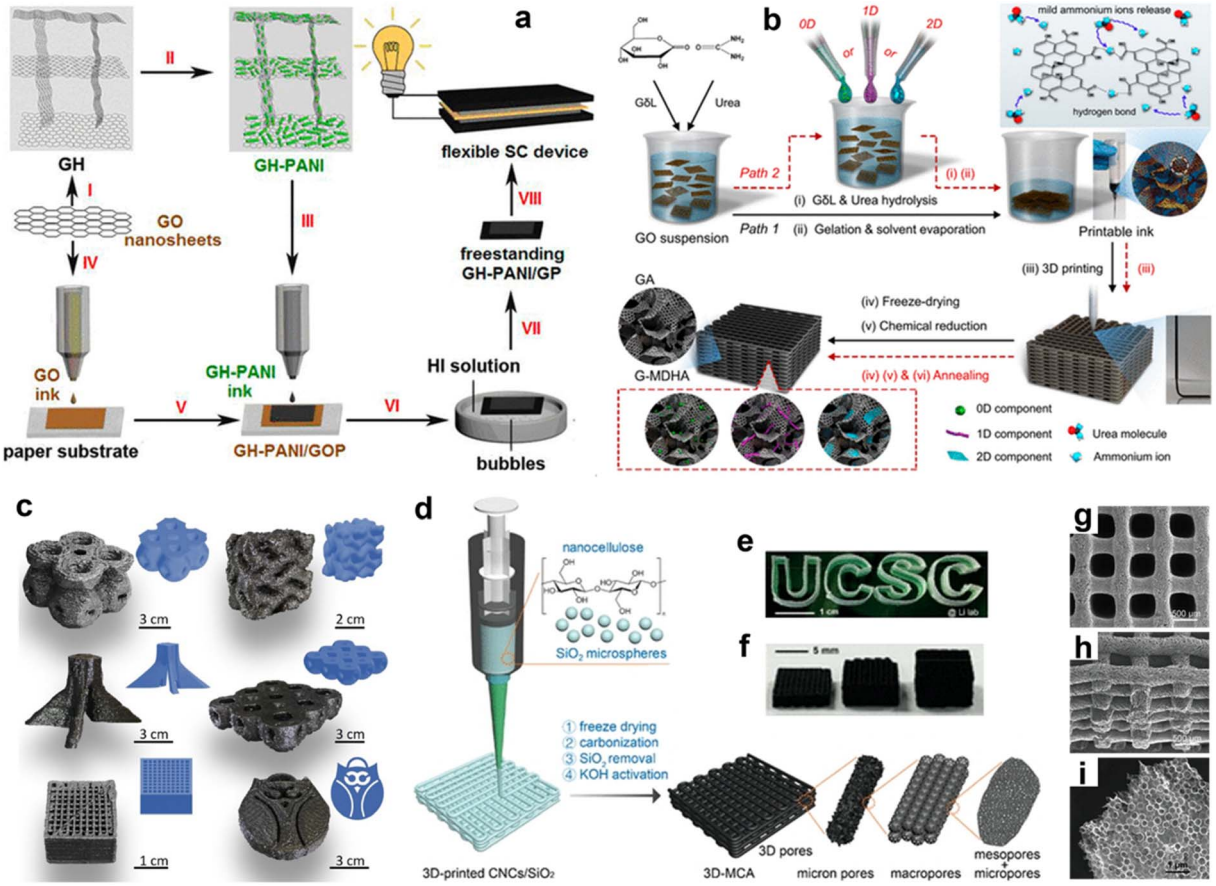

Fig. 7 (a) Fabrication scheme of a graphene hydrogel–polyaniline composite. Reproduced with permission.[129] Copyright 2014, American Chemical Society. (b) 3D printing of graphene-based mixed-dimensional hybrid aerogels. Reproduced with permission.[131] Copyright 2018, American Chemical Society. (c) 3D-printed various complex structures. Reproduced with permission.[132] Copyright 2021, Elsevier. (d) Schematic fabrication of 3D multiscale porous carbon aerogels (3D-MCA) and their digital image with (e) a shape of "UCSC" and (f) various thicknesses. (g) Top-view, (h) cross-sectional, and (i) fringe-sectional SEM images of 3D-MCA. Reproduced with permission.[134] Copyright 2021, American Chemical Society.

outstanding thermal, electrical, and mechanical performances, and the clay additive did not change these properties, resulting from the good interlayer dispersion and mixing within graphite materials.

Furthermore, the structural engineering of carbon architectures through additive manufacturing techniques with specific ink components is a feasible route to expedite the kinetics of ion diffusion and electron transport, which would allow energy-storage devices to operate at low temperatures. Li's group printed 3D-MCA *via* combining chemical methods and direct ink writing technology,[134] using a homogeneous and high viscosity ink made of cellulose nanocrystals and a silica microsphere suspension (Fig. 7d). Sophisticated shapes could be obtained by direct 3D printing and these kept well in the air (Fig. 7e). Multiscale geometries and pore architectures with various thicknesses were prepared after carbonization of the freeze-dried printed lattices, SiO_2 elimination, and KOH activation (Fig. 7f). The printed 3D carbon aerogels clearly exhibited periodic pores (~500 μm in diameter) in the layer-by-layer woodpile architecture (Fig. 7g and h). The carbon flakes in each ligament consisted of interlaced cavities (Fig. 7i). Such a well-developed open structure guaranteed the effective penetration of the electrolyte into the deep internal spaces of the carbon electrodes, giving the 3D-printed carbon aerogel enhanced electrochemical capacitive performances when working at low temperature in comparison to its non-3D-printed counterpart.

Briefly, this section introduces six design methods for carbon superstructures, which are systemically summarized and compared in Table 1, including the typical structures, synthetic features, and advantages and disadvantages of each synthetic strategies. These versatile strategies endow the carbon superstructures with a wide tunability of morphologies, pore-structure parameters, and functionalities. Based on the respective characteristics of the existing technologies, these should be comprehensively considered to develop more efficient, sustainable, and customizable synthetic routes to achieve the precise control of high-quality carbon superstructures toward large-scale and practical applications.

Table 1 Comparison of the design methods for carbon superstructures

Methods	Typical structures	Synthetic features	Advantages	Disadvantages
Hydrothermal approach	Chestnut shells Spherical particles Flowers Hydrangeas Tube-sheet arrays	Sealed pressure vessel, high pressure or temperature	Facile manipulation; easy processability; uniform structures; wide applicability	High equipment demand; strict technology; poor operation safety
Templating method	Macroporous arrays Sphere-in-tubes Mesoporous spheres Macroporous nanoshells Asymmetric flasks	Use of soft/hard templates	Controllable geometries; high-quality structures; easy production; wide applicability	Template removal; time consuming; relative high cost; low yield
Nanoemulsion assembly	Mesoporous spheres Mesopore arrays Gradient-pore core–shells Spiral supraparticles Bowl-like particles	Dependent on liquid–liquid interface interaction	Tunable dimensions and geometries; accessible anisotropic hierarchical structures	Complex operations; sensitive to experimental conditions; low yield
Spatially confined assembly	Orderly aligned opals multichamber microspheres Grid-like microspheres	Controlling the polymerization in a confined space	Designable spherical geometries and interior chambers	Limited structure category; complex interactions among precursors
Modular self-assembly	Layer superstructures Microflowers Nanotentacle structures Ordered nanoparticle arrays	Spontaneous “bottom-up” self-assembly process	Facile manipulation; easy processability; high yield; large-scale production	Sensitive to experimental conditions; hard control of structure regularity
Direct ink writing	Freestanding graphene Multi-dimensional aerogels Sophisticated structures Layer-by-layer architectures	Use of a computer-controlled translation stage	Precise shape design; large-scale production; easy processability; without expensive tools	Limited ink category; low printing resolution; poor mechanical properties of carbon materials

3. Carbon superstructures for energy storage

3.1 Supercapacitors

Supercapacitors show significant merits as energy-storage devices, including a fast charge/discharge rate (within seconds), high power output, ultralong service life, wide working temperature range, and high safety.[135–138] These desirable features give supercapacitors great application prospects in portable electronics, large industrial-scale systems, and hybrid-electric vehicles.[139–142] Carbon materials are the most widely applied supercapacitor electrodes due to their good conductivity, large surface area, and easy-adjustable pore environments.[143–145] For carbon-based supercapacitors, an ideal carbon electrode should feature an ordered morphology, rational pore-structure parameters, and heteroatomic functions to promote an enhancement of the charge-storage properties.[144,146]

Compared with the currently used porous carbons, carbon superstructures with well-defined geometries and exposed electroactive motifs enable them to serve as desirable platforms for exploring the ion-uptake/removal behaviors during supercapacitor electrochemistry. Feng and coworkers reported hierarchical superstructural carbons originating from the assembly of polyimide nanosheets with a thickness of 15 nm (Fig. 8a).[32] The flower-like carbon superstructures with a large exposed surface area (1375 $m^2 g^{-1}$) and N content (3.46 wt%) delivered a high capacitance of 364 F g^{-1} at 0.6 A g^{-1} and ~100% capacitance retention over 10 000 cycles at 10 A g^{-1} for carbon-based supercapacitors using KOH electrolyte (Fig. 8b and c), which surpassed many previously reported carbon devices. Carbon superstructures with locally graphitized configurations that could boost the conductivity and stability of bulk frameworks have been also actively investigated as potential electrode materials for supercapacitors.[147] As an example, guided by the hydrothermal self-assembly strategy, uniform hydrangea-like multiscale hollow submicron carbon spheres built of partially graphitized carbon nanosheets were prepared (Fig. 8d and e).[55] Thanks to the large surface area (934 $m^2 g^{-1}$) and open micro-/mesopores (0.6–6 nm), as-prepared carbon hydrangeas as supercapacitor electrodes could stably store/release charge for 5000 cycles at 5 A g^{-1} (Fig. 8f), validating the outstanding long-lasting cyclic stability.

As has been well-established, the synchronous introduction of high-level heteroatoms and a large surface area into stable carbon superstructures helps to elevate the physical adsorption and chemical redox processes of charge carriers for achieving double-high supercapacitive activity and durability.[148,149] Tan and coworkers designed N/O co-doped carbon nanocages with a human brain-like winkle shape (Fig. 8g and h), high N/O content (16.24/5.36 at%), and large surface area (813 $m^2 g^{-1}$).[150] When evaluated as electrode materials for supercapacitors, the superstructural carbons presented a high capacitance of 311.1 F g^{-1} at 0.5 A g^{-1} and an excellent rate capability of 118.1 F g^{-1} at 30 A g^{-1}, together with superior cycling stability, showing 97.6% capacitance retention after 10 000 cycles at 10 A g^{-1} in KOH electrolyte (Fig. 8i). Such a structural/functional synergy effect was also exemplified by

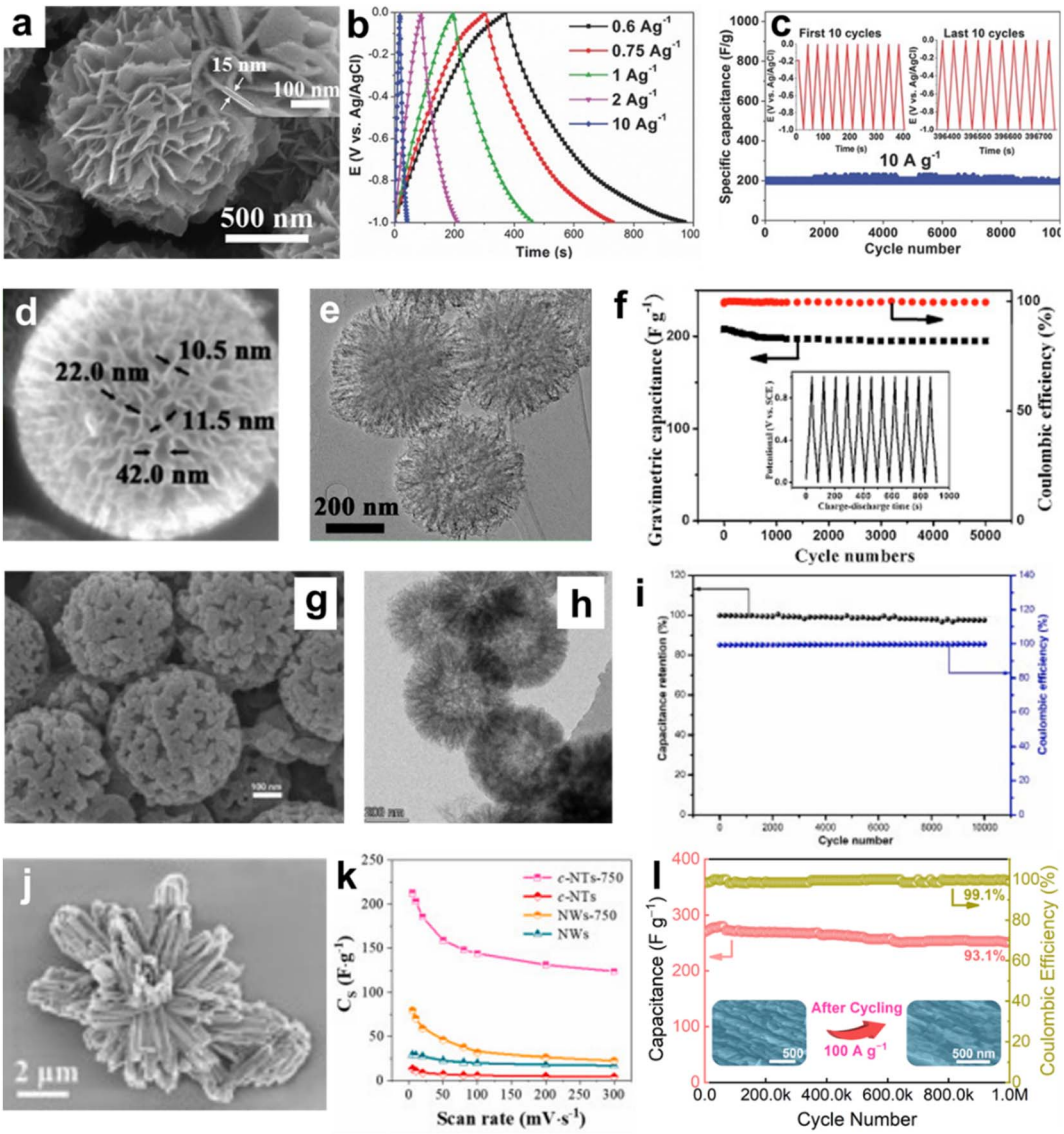

Fig. 8 (a) SEM image, (b) galvanostatic charge–discharge curves, and (c) cycling stability of porous carbon superstructures. Reproduced with permission.[32] Copyright 2016, Wiley-VCH. (d) SEM image, (e) TEM image, and (f) cycle life of carbon hydrangeas. Reproduced with permission.[55] Copyright 2015, Elsevier. (g) SEM image, (h) TEM image, and (i) stability of wrinkled carbon nanocages. Reproduced with permission.[150] Copyright 2021, Elsevier. (j) SEM image and (k) rate performance of hybrid C_{60} superstructures. Reproduced with permission.[151] Copyright 2023, Elsevier. (l) Durability over one million cycles of carbon superstructures (inset: SEM images before and after cycling). Reproduced with permission.[38] Copyright 2021, Wiley-VCH.

crossed-tubular fullerene hybrid crystals through a modified liquid–liquid interfacial precipitation method (Fig. 8j).[151] High-temperature calcination converted these hybrid crystals into mesoporous hollow carbon superstructures with an improved surface area (432.41 $m^2\ g^{-1}$) and rich self-doping oxygen heteroatoms, giving the fabricated supercapacitor a high-rate capacitance of 124 F g^{-1} at 300 mV s^{-1} (Fig. 8k). These studies shed light on structural/functional engineering for carbon superstructures toward efficient energy storage.

Of note, crafting heterogeneous active sites within carbon frameworks provides great potential to break the energy limitation of supercapacitors, but the presence of abundant heteroatomic motifs can essentially degenerate the scaffold firmness and electrochemistry kinetics.[38] Thus, the assembled supercapacitors fail to realize the theoretical millions of cycles. Presently, the cycle life of carbon-based supercapacitors reported so far rarely exceeds 200 000 cycles, especially at large current densities.[148] To deal with this dilemma, our group designed laminated carbon superstructures built of nanoparticle modules (Fig. 8l).[38] The reduced uptake energy and improved charge-density distribution in our as-prepared carbon superstructures promoted a high accessibility of the built-in protophilic sites and efficient ion migration with low energy barriers. Such carbon superstructures thus showed ultrastable and rapid proton-coupled charge-storage kinetics at the structural–chemical defects, contributing to a high-rate

Table 2 Summary of various carbon superstructures as electrode materials for supercapacitors

Geometries	Surface area ($m^2\ g^{-1}$)	Pore size (nm)	Heteroatom (wt%)	Capacitance (F g^{-1}@A g^{-1})	Lifespan%@cycle@A g^{-1}	Ref.
Carbon flowers	1375	1.6/1.9/3.9	N: 3.46; O: 7.99	364@0.6; 200@10	100%@10 000@10	32
Laminated structures	1993	0.5–10	N: 10.22; O: 5.04	468@1; 269@100	93.1@1 000 000@100	38
Carbon flowers	796	3.9	N/A	226@0.5; 185@20	103@2000@10	52
Carbon flowers	549	0.8/1.2	O: 8.00	244@0.2; 120@60	100@20 000@5	53
Carbon hydrangeas	934	0.6–6	O: 10.0	386@0.2; 171@15	94%@5000@5	55
Carbon foams	2685	0.9/2.5/5	N: 6.71; O: 4.52	403@1; 309@100	90@30 000@20	57
Carbon bubbles	905	5.3	N: 4.61; O: 2.13	244@0.67; 139@134	98.5@10 000@20	63
Carbon flasks	2335	0.5–10	N: 0.5; O: 6.4	263@0.1; 200@20	100@10 000@20	87
Multichamber spheres	1797	0.6/1.4	N: 4.58; O: 2.12	301@0.2; 210@5	100@5000@5	100
Wrinkled nanocages	813	3.9	N: 16.24; O: 5.36	311@0.5; 118@30	97.6@10 000@10	150
Hollow nanotubes	432	3.94	N/A	158@1; 87@20	98.5@2000@5	151

survivability (100 A g^{-1}) and unprecedented lifespan (93.1% capacity retention over 1 000 000 cycles) for supercapacitors. Such excellent capacitive performances profited from the well-defined superstructure configurations, which acted as robust and frameworks during large-current electrochemistry to improve the electron transfer along the integrated networks and to facilitate ion diffusion into the electrode surfaces. The electrochemical metrics of various carbon superstructures applied in supercapacitors are systematically summarized (Table 2), indicating their great potential for application in energy storage.

3.2 Zinc-ion hybrid capacitors

Zn-ion hybrid capacitors (ZHCs), a newly-emerging energy-storage device consisting of a battery-type Zn anode and a capacitive carbon cathode, have attracted extensive attention because they integrate the respective merits of batteries and supercapacitors.[152–155] On the one hand, Zn metal is considered to be an ideal anode due to its overwhelming superiorities of a low potential (−0.76 V *vs.* standard hydrogen electrode), high theoretical capacity (820 mA h g^{-1}), natural abundance and massive production, and high safety and compatibility in aqueous electrolytes.[156,157] On the other hand, a porous carbon cathode theoretically possesses an infinite cycling life resulting from the adsorption/desorption charge-storage mechanism without chemical-phase transformation.[158–160] As a result, the fast plating/stripping process of Zn^{2+} on the Zn anode gives a battery-level energy density, while the highly reversible uptake/removal of Zn^{2+} on the carbon cathode promises a capacitor-mode power density, which creates the possibility of integrating the advantages of these two stand-alone technologies.[161–163] In view of the constant redox potential and specific capacity of Zn anode, it is highly important to explore nanostructure-specific high-performance carbon cathodes to match the Zn anode for substantially revolutionizing the energy-storage metrics of ZHCs.

Carbon superstructures with desirable topographies and functions are conducive to creating ZHCs with large-current survivability and a high energy density. For example, Hu's group designed N-enriched honeycomb-like porous carbon matrices as capacitive cathodes for ZHCs (Fig. 9a and b).[164] The hierarchical open nanoarchitectures with high-level N doping and multiscale pore channels facilitated fast ion diffusion and provided sufficient electrochemical active sites for ion adsorption, thus achieving a high-rate capability of 101.3 mA h g^{-1} at 100 A g^{-1} and an energy supply of 93.7 W h kg^{-1} for the assembled ZHCs (Fig. 9c and d). Additionally, it is advantageous to further build hierarchical mesoporous architectures within carbon superstructures to achieve a reasonably high energy density. Liu's group applied a phenolic resin as a precursor to prepare mesoporous hollow carbon spheres (Fig. 9e and f).[165] When used as ZHC electrodes, the mesoporous hollow nanostructures of carbon spheres provided better double-layer capacitive properties and inhibited the growth of Zn dendrites on the Zn anode, contributing to highly reversible electrochemical capacities at various current rates, as well as an energy density of 129.3 W h kg^{-1} and a superb power output of 13.7 kW kg^{-1} (Fig. 9g and h).

The electroactive carbons with sophisticated multi-dimensional structures also play a crucial role in Zn-ion-storage metrics.[166,167] Taking a recent work as an example, Ruoff's group designed a necklace-like hollow tubular MOF-derived carbon architecture by growing microporous ZIF-8 particles and a uniform layer of ZIF-8 on sacrificial ZnO tetrapods (Fig. 9i).[168] This 3D hollow necklace architecture with continuous core–shell arms and highly porous polyhedral particles proved beneficial over physically attached or embedded particle-nanotube/nanowire systems due to its consecutive electron-conduction paths and unblocked porous structures. Consequently, the fabricated ZHCs delivered an extremely high energy density of 189.6 W h kg^{-1} and a remarkable cycle performance of 80.5% capacity retention after 10 000 cycles (Fig. 9j and k). Very recently, a nanotentacle-constructed carbon superstructure was designed (Fig. 9l and m) and the fabricated ZHCs harvested a high-energy density of 161.2 W h kg^{-1} and a prodigious lifespan of 96.8% capacity retention after 400 000 cycles (Fig. 9n and o),[114] exceeding reported Zn-ion devices in terms of all-round performances. The combination of theoretical calculations and experimental analysis ascribed the working mechanism of carbon superstructures to opposite charge-carrier adsorption coupled with the redox reaction, entailing the alternate binding of Zn^{2+}/

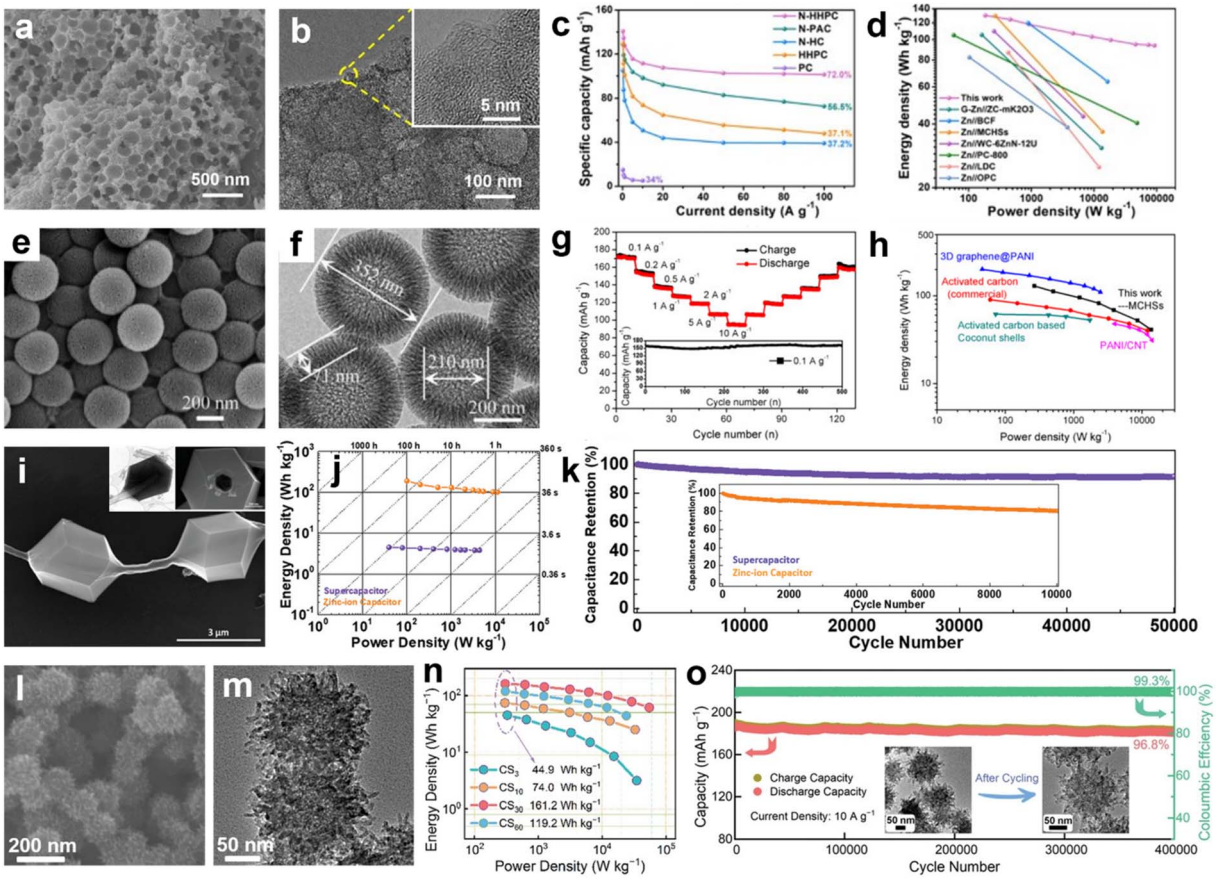

Fig. 9 (a) SEM image and (b) TEM image of the honeycomb-like carbon matrix. (c) Rate performance and (d) Ragone plots of the assembled Zn-ion hybrid capacitors. Reproduced with permission.[164] Copyright 2022, Elsevier. (e) SEM image and (f) TEM image of mesoporous hollow carbon spheres and their (g) rate performance and (h) Ragone plot for Zn-ion capacitors. Reproduced with permission.[165] Copyright 2020, Elsevier. (i) SEM image, (j) Ragone plots, and (k) cycling performance of a necklace-like tubular 3D carbon framework cathode. Reproduced with permission.[168] Copyright 2020, Wiley-VCH. (l) SEM image and (m) TEM image of carbon superstructures and corresponding (n) Ragone plots and (o) cyclability. Reproduced with permission.[114] Copyright 2022, Wiley-VCH.

$CF_3SO_3^-$ at the zincophilic sites and the chemical interaction between Zn^{2+} and carbonyl/pyridine motifs to form O–Zn–N bonds. These illustrational studies exhibit the successful implementation of Zn-ion devices based on carbon superstructures. For clarity, some diverse carbon superstructures as cathode materials for use in Zn-ion hybrid capacitors are summarized in Table 3.

3.3 Batteries

Profiting from their integrative networks and desirable pore structures, carbon superstructures are capable of facilitating ion diffusion/insertion within electrodes, which affords boosted redox kinetics and a higher reversible capacity.[169–171] Meanwhile, rich heteroatomic motifs throughout the superstructure scaffold can optimize the localized electrons near the

Table 3 A summary of diverse carbon superstructures as cathode materials for zinc-ion hybrid capacitors

Geometries	Surface area ($m^2\ g^{-1}$)	Pore size (nm)	Heteroatom (wt%)	Capacity (mA h g^{-1}@A g^{-1})	Lifespan%@cycle@A g^{-1}	Ref.
Laminated structures	1993	0.5–10	N: 10.22; O: 5.04	198@0.5; 120@50	91.8@200 000@40	38
Hierarchical spheres	789	1.0; 4.1; 8.2	N: 4.32; O: 5.01	180@0.5; 58@100	98.2@50 000@5	78
Nanotentacle structures	1522	0.5; 0.7; 3.1	N: 4.52; O: 4.95	265@0.5; 112@100	96.8@400 000@10	114
Open carbon cages	1733	1.5; 3.5; 75	N: 1.84; O: 5.82	225@0.1; 70@20	96.5@300 000@50	154
Honeycomb carbons	685	1.9; 4.7	N: 13.5; O: 13.7	141@0.2; 101@100	82.4@40 000@5	164
Mesoporous spheres	1275	1.2; 4.6; 10.7	N/A	175@0.1; 97@10	96@10 000@1	165
Honeycomb carbons	3525	2–4	O: 4.0	231@0.5; 119@20	70@18 000@10	166
Carbon flowers	1307	0.6; 2.73	N: 3.95; O: 5.85	188@0.5; 121@20	100.5@20 000@35	167
Necklace-like carbons	844	1.0	N: 9.7; O: 3.9	190@0.1; 101@10	80.5@10 000@5	168

heteroatoms, and upgrade the material conductivity and faradaic nature for enhanced cycling stability.[172,173] These merits make carbon superstructures promising candidates for advanced energy-storage batteries.

Recently, Zou's group prepared a nanorod-assembled MOF superstructure as a precursor to fabricate a 3D carbon superstructure with preserved morphology as an anode material in K-ion batteries (Fig. 10a and b),[174] in which the abundant micropores and nitrogen doping afforded a sufficient charge-storage space and rapid electron-transfer rate, thus achieving high-capacity (305 mA h g^{-1}) and long-life (500 cycles) K-ion storage (Fig. 10c). Zhao's group reported the anisotropic self-assembly of asymmetric mesoporous carbon hemispheres with a jellyfish-like shape and radial multilocular mesostructure (Fig. 10d and e).[175] Exposed active sites on peculiar core–shell architecture of carbon hemispheres ensured high-speed ion transport to the accessible electrode surface, empowering their applied as a high-performance anode with high reversible capacity of 364 mA h g^{-1} and excellent capacitive contribution of 81% at 1 mV s^{-1} for Na-ion batteries (Fig. 10f and g). This result confirmed the geometry and microstructure superiorities of the jellyfish-like carbon hemispheres.

Furthermore, carbon superstructures have been also studied as an ideal conductive matrix to load low-conductivity sulfur or organics to boost the electrochemical reaction kinetics of batteries and to achieve a higher utilization of the redox-active sites of electrodes. As an example, Bao's group infiltrated sulfur into nanostructured carbon flowers to obtain stable S/carbon composites for Li–S batteries (Fig. 10h).[176] The exposed and interlaced flower petal structure provided fast diffusion pathways and tolerated the volume change of the interior S species, allowing stable and efficient sulfur redox cycling (Fig. 10i). Qiao's group synthesized multi-layered mesoporous hollow carbon nanospheres as the sulfur host cathode material.[82] The multi-shelled carbon architectures supplied open active diffusion channels, thus achieving a high-capacity delivery of 1200 mA h g^{-1} at 0.09C for the assembled Li–S battery. Aiming at low conductivity and the inevitable dissolution of small-molecule organics in aqueous electrolytes, our group encapsulated dinitrobenzene molecules in nanostructured carbon flowers based on a facile melt-diffusion strategy to fabricate insoluble organic/carbon vehicles with a retained intactness of the nitro groups (Fig. 10j),[177] obtaining a Zn–organic battery with a superior cycling stability for up to 25 000 cycles at 5 A g^{-1}. As a proof-of-concept application, Table 4 shows some typical examples of versatile carbon superstructures as electrode materials, and the successful introduction of active organics into superstructure containers to form good

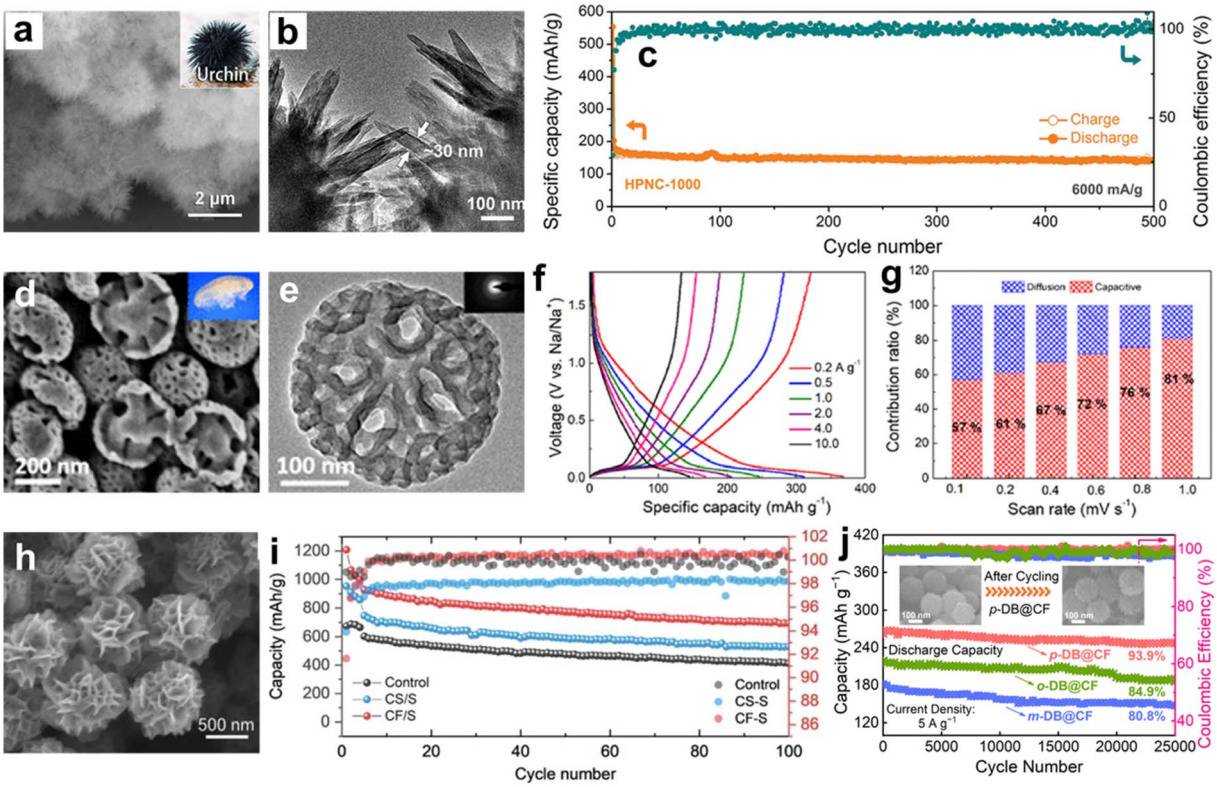

Fig. 10 (a) SEM image, (b) TEM image, and (c) cycle stability of nanorod-assembled carbon superstructure anodes for K-ion batteries. Reproduced with permission.[174] Copyright 2021, Wiley-VCH. (d) SEM image and (e) TEM image of asymmetric mesoporous carbon hemispheres and their (f) rate capabilities and (g) capacity contribution ratios in Na-ion batteries. Reproduced with permission.[175] Copyright 2022, American Chemical Society. (h) SEM image of carbon flowers and corresponding (i) capacity retention in Li–S batteries. Reproduced with permission.[176] Copyright 2021, Wiley-VCH. (j) Cycle stability of dinitrobenzene-hosted carbon nanoflower cathodes in Zn–organic batteries. Reproduced with permission.[177] Copyright 2022, Wiley-VCH.

Table 4 Summary of some versatile carbon superstructures as electrodes or host materials for batteries

Geometries	Surface area (m^2 g^{-1})	Pore size (nm)	Heteroatom (wt%)	Capacity (mA h g^{-1}@A g^{-1})	Lifespan%@cycle@A g^{-1}	Applications	Ref.
Carbon flowers	654	2.5	N/A	464@0.5	69.2@5500@5	K-ion batteries	169
Superstructures	1372	0.7; 1.1	N/A	666@0.1	82.7@100@0.1	K-ion batteries	170
Superstructures	915	0.55; 1–2	N: 8.32	305@0.6	100@500@6	K-ion batteries	174
Hemispheres	684	14	N: 6.3; O: 7.5	431@0.1	78@1000@5	K-ion batteries	175
Multilayers	857	3.5	N/A	1200@0.09C	100@30@1.8C	Li–S batteries	82
Superstructures	363	0.9; 4	N: 4.6	755@2C	99.6@1500@1	Li–S batteries	171
Carbon flowers	3300	<2	N: 1.5; O: 7.0	1208@0.05C	69.8@100@0.1C	Li–S batteries	176
Carbon flowers	672	0.6; 2–8	O: 3.06	402@0.1	93.9@25 000@5	Zn-ion batteries	177

contacts and well-defined nanocomposite electrodes for advanced batteries.

Briefly, the above-mentioned section highlights the promising applications of versatile carbon superstructures as electrode materials for achieving efficient energy-storage performances in terms of the specific capacity, rate capability, and cycle life. Extensive efforts have been made to obtain a clear knowledge of the relationship between the structural attributes and electrochemical metrics of carbon superstructures. It has been well-established that the geometry, pore-structure parameters, and heteroatom doping are particularly critical factors for the electrochemical energy storage of carbon superstructures. First, well-arranged integrative carbon superstructures afford abundant exposed surface-active motifs, robust skeletons with excellent mechanical strength, and continuous electron-transfer routes, triggering enhanced reaction kinetics and charge storage. Second, the large surface area provides abundant interaction platforms for the reversible uptake/removal of charge carriers, while the hierarchical porosity stimulates fast ion diffusion and a high accessibility of the built-in electroactive sites with low energy barriers. Third, the implantation of heterogeneous heteroaromatic sites (such as N, O, P, and S species) into carbon scaffolds upgrades the electrolyte/electrode interface compatibility, the surface accessibility, and the faradaic response for ensuring durable supercapacitive activity in electrochemical-sensitive procedures. Therefore, it is highly desirable to build multifunction-coupled 3D carbon superstructures that integrate a well-defined topology, ingenious multiscale hierarchy, and favorable functional attributes for substantially unlocking superior device performances to meet the increasing energy-storage targets of today and the future.

4. Summary and outlook

Carbon superstructures have drawn growing interest for energy applications due to their various synthesis strategies and the wide tunability of their structural and functional properties. To fulfill the urgent demands of advanced energy-storage devices, significant efforts have been made to explore high-performance carbon superstructures as electrode materials. A variety of carbon superstructures, such as flowers, tube-sheet arrays, flasks, nanocages, hydrangea, honeycombs, necklaces, hemispheres, multi-shelled hollow, and virus-like structures, have been facilely designed by regulating the synthesis conditions. In this review, we summarized the recent achievements in the design, synthesis, and understanding the mechanisms of 3D carbon superstructures, which will help to establish a predictive model for constructing versatile carbon superstructures with on-demand and precise control. The potential applications of carbon superstructures in the energy-storage fields were also highlighted, which provides the useful framework for understanding the structure–performance relationships. This is significant to drive chemistry science, nanomaterial science, and crossover fields. Despite significant progress being made, some important aspects and opportunities for the future research of carbon superstructures need to be considered, as set out below.

(1) Establishing a comprehensive synthetic method and theory for the controlled and on-demand construction of carbon superstructures. To date, it has been difficult to unify the knowledge from existing studies for the fabrication of carbon superstructures with different structural arrangements, components, pore architectures, and morphologies because of the high susceptibility of the self-assembly process, which can lead to variations. There thus remains a need to precisely synthesize well-aligned carbon superstructures with targeted geometries and functionalities, and that is what we demand. It is thus important to gain a better understanding of the underlying mechanisms in the oriented self-assembly of carbon precursors. For example, recent achievements based on modular self-assembly mechanisms are very promising but are still in their early stage. Although the self-assembly process can be well governed when applying well-organized low-dimensional modules as structure-oriented units instead of traditional block copolymers/surfactant molecules, the resulting carbon superstructures have remained limited to spherical architectures. The key step is the creation of novel building blocks with non-spherical shapes for oriented modular assembly into exquisite multilevel architectures.

(2) Improving the printing resolution of DIW technology and developing versatile DIW inks. DIW technology does well in engineering large-pore structures in 3D carbons, but it is incapable of designing the structural parameters of the meso-/micropores. Boosting the printing resolution is highly needed to shape DIW into a powerful protocol for electrode manufacturing. Furthermore, diversified electrochemical active

materials (not limited to graphene aerogels) should be developed as DIW inks for the production of complex carbon superstructures with unique pore alignments and multiple functions. For example, the conversion of biomass precursors into printable inks may be a prospective direction for future exploration for the ever-growing energy applications.

(3) Mass fabrication of carbon superstructures with targeted compositions and well-formed architectures toward practical applications. Although many significant attempts have been made to explore the future applications of carbon superstructures, their scalable, reproducible, and cost-effective manufacture with well-maintained physicochemical features are still challenging. Of note, most the reported excellent properties of carbon superstructure-based devices have been obtained with a low mass loading of active materials in the electrodes (<2 mg cm^{-2}), which is far away from the commercial level needed ($\geq$10 mg cm^{-2}). It is thus of great importance to devise new techniques and tailor-made platforms to maintain the promising electrochemical performance metrics of carbon superstructures under high-mass-loading conditions to match the urgent and key demands of energy-storage devices in terms of sustainability and industrialization. Therefore, continuous efforts are imperative to extend the production scale of emerging sustainable carbon superstructures from the laboratory stage to the practical industrial level.

(4) In-depth understanding of the structure–property relationships and potential mechanisms in carbon superstructures. Carbon superstructures have substantially promoted the progress in energy-storage and energy-conversion technologies. However, the relationships between superstructures and their excellent electrochemical properties remains to be thoroughly studied. The use of theoretical calculations and advanced *in*/*ex situ* spectroscopy techniques as powerful tools can be carried out to give additional fundamental insights for understanding the host–guest interactions as well as their electrochemical reaction mechanisms, but these are not enough. These aspects for material fabrication should be considered too in order to provide guidance for superstructure design toward their emerging applications.

(5) Close combination of the favorable properties of carbon superstructures to match the actual needs. The key to further expanding the special application field of functional carbon superstructures is how to closely to combine the unique superiorities of the materials with the real requirements. For example, how to achieve precise regulation over the geometry and pore structure at the nanoscale to meet the battery application requirements involving ion-diffusion/uptake kinetics. With increasing efforts devoted to this area, the achievements from related studies will guide the design of desirable multileveled carbon superstructures with beneficial functionalities and remarkable electrochemical metrics. We expect that carbon superstructures will continue to bring significant breakthroughs in energy-related realms.

Conflicts of interest

The authors declare no competing financial interest.

Acknowledgements

This work is financially supported by the National Natural Science Foundation of China (No. 22272118, 22172111, 21905207, and 21875165), the Science and Technology Commission of Shanghai Municipality, China (No. 22ZR1464100, 20ZR1460300, and 19DZ2271500), China Postdoctoral Science Foundation (2022M712402), Zhejiang Provincial Science and Technology Project (2022C01182), and the Fundamental Research Funds for the Central Universities (22120210529).

References

1 E. Zhang, Y.-C. Wu, H. Shao, V. Klimavicius, H. Zhang, P.-L. Taberna, J. Grothe, G. Buntkowsky, F. Xu, P. Simon and S. Kaskel, *J. Am. Chem. Soc.*, 2022, **144**, 14217–14225.
2 W. Chen, J. Gu, Q. Liu, M. Yang, C. Zhan, X. Zang, T. A. Pham, G. Liu, W. Zhang, D. Zhang, B. Dunn and Y. Morris Wang, *Nat. Nanotechnol.*, 2022, **17**, 153–158.
3 Y. Gogotsi and P. Simon, *Science*, 2018, **334**, 917–918.
4 J. He, C. Lu, H. Jiang, F. Han, X. Shi, J. Wu, L. Wang, T. Chen, J. Wang, Y. Zhang, H. Yang, G. Zhang, X. Sun, B. Wang, P. Chen, Y. Wang, Y. Xia and H. Peng, *Nature*, 2021, **597**, 57–63.
5 L. Ye, Y. Hong, M. Liao, B. Wang, D. Wei, H. Peng, L. Ye, Y. Hong, M. Liao, B. Wang, D. Wei and H. Peng, *Energy Storage Mater.*, 2020, **28**, 364–374.
6 W. Guo, C. Yu, S. Li, X. Song, H. Huang, X. Han, Z. Wang, Z. Liu, J. Yu, X. Tan and J. Qiu, *Adv. Mater.*, 2019, **31**, 1901241.
7 Y. Kong, C. Tang, X. Huang, A. K. Nanjundan, J. Zou, A. Du and C. Yu, *Adv. Funct. Mater.*, 2021, **31**, 2010569.
8 Y. Yang, P. Zhang, L. Hao, P. Cheng, Y. Chen and Z. Zhang, *Angew. Chem., Int. Ed.*, 2021, **60**, 21838–21845.
9 Z. Wu, S. Xu, Q. Yan, Z. Chen, Y. Ding, C. Li, H. Liang and S. Yu, *Sci. Adv.*, 2018, **4**, eaat0788.
10 J. Yu, C. Yu, W. Guo, Z. Wang, S. Li, J. Chang, X. Tan, Y. Ding, M. Zhang, L. Yang, Y. Xie, R. Fu and J. Qiu, *Nano Energy*, 2019, **64**, 103921.
11 J. Wang, Y. Yao, C. Zhang, Q. Sun, D. Cheng, X. Huang, J. Feng, J. Wan, J. Zou, C. Liu and C. Yu, *Adv. Sci.*, 2021, **8**, 2100120.
12 C. Liu, X. Huang, J. Wang, H. Song, Y. Yang, Y. Liu, J. Li, L. Wang and C. Yu, *Adv. Funct. Mater.*, 2018, **28**, 1705253.
13 Y. Zhang, G. Li, J. Wang, D. Luo, Z. Sun, Y. Zhao, A. Yu, X. Wang and Z. Chen, *Adv. Energy Mater.*, 2021, **11**, 2100497.
14 W. Zhang, M. Sun, J. Yin, K. Lu, U. Schwingenschlögl, X. Qiu and H. N. Alshareef, *Adv. Energy Mater.*, 2021, **11**, 2101928.
15 L. Dong, X. Ma, Y. Li, L. Zhao, W. Liu, J. Cheng, C. Xu, B. Li, Q.-H. Yang and F. Kang, *Energy Storage Mater.*, 2018, **13**, 96–102.
16 H. He, J. Lian, C. Chen, Q. Xiong, C. C. Li and M. Zhang, *Nano-Micro Lett.*, 2022, **14**, 106.
17 Y. Zhao, Y. Zhang, Y. Wang, D. Cao, X. Sun and H. Zhu, *Carbon Energy*, 2021, **3**, 895–915.

18 C. Li, W. Wu, P. Wang, W. Zhou, J. Wang, Y. Chen, L. Fu, Y. Zhu, Y. Wu and W. Huang, *Adv. Sci.*, 2019, **6**, 1801665.
19 L. Wu and Y. Dong, *Energy Storage Mater.*, 2021, **41**, 715–737.
20 H. Wang, Y. Shao, S. Mei, Y. Lu, M. Zhang, J. K. Sun, K. Matyjaszewski, M. Antonietti and J. Yuan, *Chem. Rev.*, 2020, **120**, 9363–9419.
21 L.-F. Chen, Y. Feng, H.-W. Liang, Z.-Y. Wu and S.-H. Yu, *Adv. Energy Mater.*, 2017, **7**, 1700826.
22 K. S. Kumar, N. Choudhary, Y. Jung and J. Thomas, *ACS Energy Lett.*, 2018, **3**, 482–495.
23 Y. Li, S. Wu, L. Zhang, X. Xu, Y. Fang, J. Yi, J. Kim, B. Shen, M. Lee, L. Huang, L. Zhang, J. Bao, H. Ji and Z. Huang, *Angew. Chem., Int. Ed.*, 2020, **59**, 21525–21529.
24 F. Wang, Q. Wang, S. Wang, K. Zhang, S. Jia, J. Chen and X. Wang, *ACS Nano*, 2022, **16**, 9049–9061.
25 W. Yang, J. Zhou, S. Wang, Z. Wang, F. Lv, W. Zhang, W. Zhang, Q. Sun and S. Guo, *ACS Energy Lett.*, 2020, **5**, 1653–1661.
26 X. Liu, F. Liu, J. Yu, G. Xiong, L. Zhao, Y. Sang, S. Zuo, J. Zhang, H. Liu and W. Zhou, *Adv. Sci.*, 2020, **7**, 2001526.
27 Y. Sun, H. Wang, W. Wei, Y. Zheng, L. Tao, Y. Wang, M. Huang, J. Shi, Z. C. Shi and D. Mitlin, *ACS Nano*, 2021, **15**, 1652–1665.
28 F. Yue, G. Gao, F. Li, Y. Zheng and S. Hou, *Carbon*, 2018, **134**, 112–122.
29 M. Wang, X. Mao, J. Liu, B. Deng, S. Deng, S. Jin, W. Li, J. Gong, R. Deng and J. Zhu, *Adv. Sci.*, 2022, **9**, 2202394.
30 K. Shen, L. Zhang, X. Chen, L. Liu, D. Zhang, Y. Han, J. Chen, J. Long, R. Luque, Y. Li and B. Chen, *Science*, 2018, **359**, 206–210.
31 M. P. Zhuo, G. P. He, X. D. Wang and L. S. Liao, *Nat. Commun.*, 2021, **12**, 2252.
32 Z. Xu, X. Zhuang, C. Yang, J. Cao, Z. Yao, Y. Tang, J. Jiang, D. Wu and X. Feng, *Adv. Mater.*, 2016, **28**, 1981–1987.
33 Y. Song, X. Song, X. Wang, J. Bai, F. Cheng, C. Lin, X. Wang, H. Zhang, J. Sun, T. Zhao, H. Nara, Y. Sugahara, X. Li and Y. Yamauchi, *J. Am. Chem. Soc.*, 2022, **144**, 17457–17467.
34 L. Tang, T. Vo, X. Fan, D. Vecchio, T. Ma, J. Lu, H. Hou, S. C. Glotzer and N. A. Kotov, *J. Am. Chem. Soc.*, 2021, **143**, 19655–19667.
35 L. Zou, C. Hou, Q. Wang, Y. Wei, Z. Liu, J. Qin, H. Pang and Q. Xu, *Angew. Chem., Int. Ed.*, 2020, **59**, 19627–19632.
36 S. Chen, D. M. Koshy, Y. Tsao, R. Pfattner, X. Yan, D. Feng and Z. Bao, *J. Am. Chem. Soc.*, 2018, **140**, 10297–10304.
37 Z. Zhao, Y. Zhao, R. Lin, Y. Ma, L. Wang, L. Liu, K. Lan, J. Zhang, H. Chen, M. Liu, F. Bu, P. Zhang, L. Peng, X. Zhang, Y. Liu, C.-T. Hung, A. Dong, W. Li and D. Zhao, *Sci. Adv.*, 2022, **8**, eabo0283.
38 Z. Song, L. Miao, L. Ruhlmann, Y. Lv, D. Zhu, L. Li, L. Gan and M. Liu, *Adv. Mater.*, 2021, **33**, 2104148.
39 Z. Song, L. Miao, L. Ruhlmann, Y. Lv, L. Li, L. Gan and M. Liu, *Angew. Chem., Int. Ed.*, 2023, **62**, e202219136.
40 Y. Li, K. Xiao, C. Huang, J. Wang, M. Gao, A. Hu, Q. Tang, B. Fan, Y. Xu and X. Chen, *Nano-Micro Lett.*, 2021, **13**, 1.
41 J. Liu, N. P. Wickramaratne, S. Z. Qiao and M. Jaroniec, *Nat. Mater.*, 2015, **14**, 763–774.
42 J. Liu, S. Z. Qiao, H. Liu, J. Chen, A. Orpe, D. Zhao and G. Q. Lu, *Angew. Chem., Int. Ed.*, 2011, **50**, 5947–5951.
43 P. Qiu, B. Ma, C. T. Hung, W. Li and D. Zhao, *Acc. Chem. Res.*, 2019, **52**, 2928–2938.
44 Y. Zheng, S. Chen, K. A. I. Zhang, J. Zhu, J. Xu, C. Zhang and T. Liu, *ACS Appl. Mater. Interfaces*, 2021, **13**, 13328–13337.
45 B. Han, E. Zhang, G. Cheng, L. Zhang, D. Wang and X. Wang, *Chem. Eng. J.*, 2018, **338**, 734–744.
46 L. Xiang, S. Yuan, F. Wang, Z. Xu, X. Li, F. Tian, L. Wu, W. Yu and Y. Mai, *J. Am. Chem. Soc.*, 2022, **144**, 15497–15508.
47 M. Liu, Q. Chen, X. Cao, D. Tan, J. Ma and J. Zhang, *J. Am. Chem. Soc.*, 2022, **144**, 21683–21691.
48 Y. He, X. Zhuang, C. Lei, L. Lei, Y. Hou, Y. Mai and X. Feng, *Nano Today*, 2019, **24**, 103–119.
49 Z. Song, H. Duan, L. Miao, L. Ruhlmann, Y. Lv, W. Xiong, D. Zhu, L. Li, L. Gan and M. Liu, *Carbon*, 2020, **168**, 499–507.
50 L. Zou, M. Kitta, J. Hong, K. Suenaga, N. Tsumori, Z. Liu and Q. Xu, *Adv. Mater.*, 2019, **31**, 1900440.
51 L. Xie, X. Li, J. Deng, Y. Gong, H. Wang, S. Mao and Y. Wang, *Green Chem.*, 2018, **20**, 4596–4601.
52 J. Liang, S. Chen, M. Xie, Y. Wang, X. Guo, X. Guo and W. Ding, *J. Mater. Chem. A*, 2014, **2**, 16884–16891.
53 Z. Li, P. Yu, W. Zhong, M. Zhang, Z. Li, A. Cheng, Y. Liang, L. Miao, X. Yang and H. Zhang, *Carbon*, 2021, **176**, 1–10.
54 H. Fan, X. Hu, S. Zhang, Z. Xu, G. Gao, Y. Zheng, G. Hu, Q. Chen, T. S. AlGarni and R. Luque, *Carbon*, 2021, **180**, 254–264.
55 D. Guo, X. a. Chen, Z. Fang, Y. He, C. Zheng, Z. Yang, K. Yang, Y. Chen and S. Huang, *Electrochim. Acta*, 2015, **176**, 207–214.
56 Z. Xu, D. Lu, L. Ma, C. Lu, X. Xi, G. Zhang, R. Liu and D. Wu, *Chem. Eng. J.*, 2019, **364**, 201–207.
57 H. Peng, B. Yao, X. Wei, T. Liu, T. Kou, P. Xiao, Y. Zhang and Y. Li, *Adv. Energy Mater.*, 2019, **9**, 1803665.
58 T. Wang, F. Okejiri, Z. A. Qiao and S. Dai, *Adv. Mater.*, 2020, **32**, 2002475.
59 C.-C. Hou, L. Zou, Y. Wang and Q. Xu, *Angew. Chem., Int. Ed.*, 2020, **59**, 21360–21366.
60 H. F. Wang, L. Chen, M. Wang, Z. Liu and Q. Xu, *Nano Lett.*, 2021, **21**, 3640–3648.
61 Y. Yan, G. Chen, P. She, G. Zhong, W. Yan, B. Y. Guan and Y. Yamauchi, *Adv. Mater.*, 2020, **32**, 2004654.
62 Y. Zhai, Y. Dou, D. Zhao, P. F. Fulvio, R. T. Mayes and S. Dai, *Adv. Mater.*, 2011, **23**, 4828–4850.
63 Z. Tang, G. Zhang, H. Zhang, L. Wang, H. Shi, D. Wei and H. Duan, *Energy Storage Mater.*, 2018, **10**, 75–84.
64 G. Wang, Y. Sun, D. Li, H. W. Liang, R. Dong, X. Feng and K. Mullen, *Angew. Chem., Int. Ed.*, 2015, **54**, 15191–15196.
65 Y. Bu, T. Sun, Y. Cai, L. Du, O. Zhuo, L. Yang, Q. Wu, X. Wang and Z. Hu, *Adv. Mater.*, 2017, **29**, 1700470.
66 Y. Fang, Y. Lv, F. Gong, Z. Wu, X. Li, H. Zhu, L. Zhou, C. Yao, F. Zhang, G. Zheng and D. Zhao, *J. Am. Chem. Soc.*, 2015, **137**, 2808–2811.
67 G. Chen, Y. Yan, J. Wang, Y. S. Ok, G. Zhong, B. Y. Guan and Y. Yamauchi, *Angew. Chem., Int. Ed.*, 2020, **59**, 19663–19668.

68 H. W. Liang, X. Zhuang, S. Bruller, X. Feng and K. Mullen, *Nat. Commun.*, 2014, **5**, 4973.
69 X. Zhou, L. Chen, W. Zhang, J. Wang, Z. Liu, S. Zeng, R. Xu, Y. Wu, S. Ye, Y. Feng, X. Cheng, Z. Peng, X. Li and Y. Yu, *Nano Lett.*, 2019, **19**, 4965–4973.
70 H. He, D. Huang, Y. Tang, Q. Wang, X. Ji, H. Wang and Z. Guo, *Nano Energy*, 2019, **57**, 728–736.
71 Z. Chen, S. Ye, S. D. Evans, Y. Ge, Z. Zhu, Y. Tu and X. Yang, *Small*, 2018, **14**, 1704015.
72 M. R. Benzigar, S. N. Talapaneni, S. Joseph, K. Ramadass, G. Singh, J. Scaranto, U. Ravon, K. Al-Bahily and A. Vinu, *Chem. Soc. Rev.*, 2018, **47**, 2680–2721.
73 L. Zhang, T. Wang, T.-N. Gao, H. Xiong, R. Zhang, Z. Liu, S. Song, S. Dai and Z.-A. Qiao, *CCS Chem.*, 2020, **2**, 870–881.
74 H. Zhang, O. Noonan, X. Huang, Y. Yang, C. Xu, L. Zhou and C. Yu, *ACS Nano*, 2016, **10**, 4579–4586.
75 J. Tang, J. Liu, C. Li, Y. Li, M. O. Tade, S. Dai and Y. Yamauchi, *Angew. Chem., Int. Ed.*, 2015, **54**, 588–593.
76 J. Chen, J. Xu, S. Zhou, N. Zhao and C.-P. Wong, *Nano Energy*, 2016, **25**, 193–202.
77 Y. Liu, Z. Wang, W. Teng, H. Zhu, J. Wang, A. A. Elzatahry, D. Al-Dahyan, W. Li, Y. Deng and D. Zhao, *J. Mater. Chem. A*, 2018, **6**, 3162–3170.
78 J. Huang, L. Wang, Z. Peng, M. Peng, L. Li, X. Tang, Y. Xu, L. Tan, K. Yuan and Y. Chen, *J. Mater. Chem. A*, 2021, **9**, 8435–8443.
79 J. Tang, J. Wang, L. K. Shrestha, M. S. A. Hossain, Z. A. Alothman, Y. Yamauchi and K. Ariga, *ACS Appl. Mater. Interfaces*, 2017, **9**, 18986–18993.
80 B. Y. Guan, S. L. Zhang and X. W. D. Lou, *Angew. Chem., Int. Ed.*, 2018, **57**, 6176–6180.
81 F. Yuan, C. Shi, Q. Li, J. Wang, D. Zhang, Q. Wang, H. Wang, Z. Li, W. Wang and B. Wang, *Adv. Funct. Mater.*, 2022, **32**, 2208966.
82 J. Liu, T. Yang, D.-W. Wang, G. Q. Lu, D. Zhao and S. Z. Qiao, *Nat. Commun.*, 2013, **4**, 2798.
83 S. C. Mei, X. H. Rui, L. Li, G. X. Huang, X. Q. Pan, M. K. Ke, Z. H. Wang, H. Q. Yu and Y. Yu, *Adv. Mater.*, 2021, **33**, 2103130.
84 L. Hou, W. C. Li, C. Y. Liu, Y. Zhang, W. H. Qiao, J. Wang, D. Q. Wang, C. H. Jin and A. H. Lu, *ACS Cent. Sci.*, 2021, **7**, 1493–1499.
85 T. Liu, F. Zhang, Y. Song and Y. Li, *J. Mater. Chem. A*, 2017, **5**, 17705–17733.
86 Z. Zhao, L. Duan, Y. Zhao, L. Wang, J. Zhang, F. Bu, Z. Sun, T. Zhang, M. Liu, H. Chen, Y. Yang, K. Lan, Z. Lv, L. Zu, P. Zhang, R. Che, Y. Tang, D. Chao, W. Li and D. Zhao, *J. Am. Chem. Soc.*, 2022, **14**, 11767–11777.
87 C. Chen, H. Wang, C. Han, J. Deng, J. Wang, M. Li, M. Tang, H. Jin and Y. Wang, *J. Am. Chem. Soc.*, 2017, **139**, 2657–2663.
88 B. Y. Guan, L. Yu and X. W. Lou, *J. Am. Chem. Soc.*, 2016, **138**, 11306–11311.
89 L. Peng, C. T. Hung, S. Wang, X. Zhang, X. Zhu, Z. Zhao, C. Wang, Y. Tang, W. Li and D. Zhao, *J. Am. Chem. Soc.*, 2019, **141**, 7073–7080.
90 L. Xie, M. Yan, T. Liu, K. Gong, X. Luo, B. Qiu, J. Zeng, Q. Liang, S. Zhou, Y. He, W. Zhang, Y. Jiang, Y. Yu, J. Tang, K. Liang, D. Zhao and B. Kong, *J. Am. Chem. Soc.*, 2022, **144**, 1634–1646.
91 Y. Liu, M. Xiao, S. Liu, X. Zhao, Y. Tian and X. Wang, *Carbon*, 2022, **200**, 361–374.
92 L. Peng, H. Peng, C.-T. Hung, D. Guo, L. Duan, B. Ma, L. Liu, W. Li and D. Zhao, *Chem*, 2021, **7**, 1020–1032.
93 D. Liu, N. Xue, L. Wei, Y. Zhang, Z. Qin, X. Li, B. P. Binks and H. Yang, *Angew. Chem., Int. Ed.*, 2018, **130**, 11065–11070.
94 L. Peng, H. Peng, Y. Liu, X. Wang, C.-T. Hung, Z. Zhao, G. Chen, W. Li, L. Mai and D. Zhao, *Sci. Adv.*, 2021, **7**, eabi7403.
95 B. C. Buddingh and J. C. M. van Hest, *Acc. Chem. Res.*, 2017, **50**, 769–777.
96 Z. Wu, W. D. Wu, W. Liu, C. Selomulya, X. D. Chen and D. Zhao, *Angew. Chem., Int. Ed.*, 2013, **125**, 14009–14013.
97 F. Pei, T. An, J. Zang, X. Zhao, X. Fang, M. Zheng, Q. Dong and N. Zheng, *Adv. Energy Mater.*, 2016, **6**, 1502539.
98 Z. Sun, Y. Liu, B. Li, J. Wei, M. Wang, Q. Yue, Y. Deng, S. Kaliaguine and D. Zhao, *ACS Nano*, 2013, **7**, 8706–8714.
99 L.-H. Zhang, B. He, W.-C. Li and A.-H. Lu, *Adv. Energy Mater.*, 2017, **7**, 1701518.
100 T. Wang, Y. Sun, L. Zhang, K. Li, Y. Yi, S. Song, M. Li, Z. A. Qiao and S. Dai, *Adv. Mater.*, 2019, **31**, 1807876.
101 P. D. Howes, S. Rana and M. M. Stevens, *Chem. Soc. Rev.*, 2014, **43**, 3835–3853.
102 Z. Nie, A. Petukhova and E. Kumacheva, *Nat. Nanotechnol.*, 2010, **5**, 15–25.
103 A. Carne-Sanchez, I. Imaz, M. Cano-Sarabia and D. Maspoch, *Nat. Chem.*, 2013, **5**, 203–211.
104 M. Zanini, C. Marschelke, S. E. Anachkov, E. Marini, A. Synytska and L. Isa, *Nat. Commun.*, 2017, **8**, 15701.
105 R. M. Erb, H. S. Son, B. Samanta, V. M. Rotello and B. B. Yellen, *Nature*, 2009, **457**, 999–1002.
106 G. Singh, H. Chan, A. Baskin, E. Gelman, N. Repnin, P. Král and R. Klajn, *Science*, 2014, **345**, 1149–1153.
107 J. Guo, B. L. Tardy, A. J. Christofferson, Y. Dai, J. J. Richardson, W. Zhu, M. Hu, Y. Ju, J. Cui, R. R. Dagastine, I. Yarovsky and F. Caruso, *Nat. Nanotechnol.*, 2016, **11**, 1105–1111.
108 M. Grzelczak, J. Vermant, E. M. Furst and L. M. Liz-Marzán, *ACS Nano*, 2010, **4**, 3591–3605.
109 V. Raeesi, L. Y. Chou and W. C. Chan, *Adv. Mater.*, 2016, **28**, 8511–8518.
110 T. Bollhorst, K. Rezwan and M. Maas, *Chem. Soc. Rev.*, 2017, **46**, 2091–2126.
111 M. A. Boles, M. Engel and D. V. Talapin, *Chem. Rev.*, 2016, **116**, 11220–11289.
112 L. Qiu, Y. Jiang, X. Sun, X. Liu and H. Peng, *J. Mater. Chem. A*, 2014, **2**, 15132.
113 W. Wang, W. Zhao, T. Chen, Y. Bai, H. Xu, M. Jiang, S. Liu, W. Huang and Q. Zhao, *Adv. Funct. Mater.*, 2021, **31**, 2010306.
114 Z. Song, L. Miao, L. Ruhlmann, Y. Lv, D. Zhu, L. Li, L. Gan and M. Liu, *Adv. Funct. Mater.*, 2022, **32**, 2208049.
115 M.-A. Shahbazi, M. Ghalkhani and H. Maleki, *Adv. Energy Mater.*, 2020, **22**, 2000033.

116 H. Zhang and A. I. Cooper, *Adv. Mater.*, 2007, **19**, 1529–1533.
117 M. C. Gutiérrez, M. L. Ferrer and F. d. Monte, *Chem. Mater.*, 2008, **20**, 634–648.
118 Y. Song, T. Liu, F. Qian, C. Zhu, B. Yao, E. Duoss, C. Spadaccini, M. Worsley and Y. Li, *J. Colloid Interface Sci.*, 2018, **509**, 529–545.
119 C. Zhu, T. Liu, F. Qian, T. Y. Han, E. B. Duoss, J. D. Kuntz, C. M. Spadaccini, M. A. Worsley and Y. Li, *Nano Lett.*, 2016, **16**, 3448–3456.
120 M. Saadi, A. Maguire, N. T. Pottackal, M. S. H. Thakur, M. M. Ikram, A. J. Hart, P. M. Ajayan and M. M. Rahman, *Adv. Mater.*, 2022, **34**, 2108855.
121 T. V. Neumann and M. D. Dickey, *Adv. Mater. Technol.*, 2020, **5**, 2000070.
122 J. A. Lewis, J. E. Smay, J. Stuecker and J. Cesarano, *J. Am. Ceram. Soc.*, 2006, **89**, 3599–3609.
123 M. Wei, F. Zhang, W. Wang, P. Alexandridis, C. Zhou and G. Wu, *J. Power Sources*, 2017, **354**, 134–147.
124 V. G. Rocha, E. Saiz, I. S. Tirichenko and E. García-Tuñón, *J. Mater. Chem. A*, 2020, **8**, 15646–15657.
125 T. Huang, W. Liu, C. Su, Y.-y. Li and J. Sun, *Nano Res.*, 2022, **15**, 6091–6111.
126 J. Roman, W. Neri, V. Fierro, A. Celzard, A. Bentaleb, I. Ly, J. Zhong, A. Derré and P. Poulin, *Nano Today*, 2020, **33**, 100881.
127 K. S. Novoselov, A. K. Geim, S. V. Morozov, D. Jiang, Y. Zhang, S. V. Dubonos, I. V. Grigorieva and A. A. Firsov, *Science*, 2004, **306**, 666–669.
128 A. K. Geim, *Science*, 2009, **324**, 1530–1534.
129 K. Chi, Z. Zhang, J. Xi, Y. Huang, F. Xiao, S. Wang and Y. Liu, *ACS Appl. Mater. Interfaces*, 2014, **6**, 16312–16319.
130 E. R. Kearns, R. Gillespie and D. M. D'Alessandro, *J. Mater. Chem. A*, 2021, **9**, 27252–27270.
131 X. Tang, H. Zhou, Z. Cai, D. Cheng, P. He, P. Xie, D. Zhang and T. Fan, *ACS Nano*, 2018, **12**, 3502–3511.
132 S. M. Sajadi, S. Enayat, L. Vásárhelyi, A. Alabastri, M. Lou, L. M. Sassi, A. Kutana, S. Bhowmick, C. Durante, Á. Kukovecz, A. B. Puthirath, Z. Kónya, R. Vajtai, P. Boul, C. S. Tiwary, M. M. Rahman and P. M. Ajayan, *Carbon*, 2021, **181**, 260–269.
133 J. Sun, C. Liu, X. Song, J. Zhang, Y. Liu, L. Liang, R. Jiang and C. Yuan, *Appl. Phys. Rev.*, 2022, **9**, 031301.
134 B. Yao, H. Peng, H. Zhang, J. Kang, C. Zhu, G. Delgado, D. Byrne, S. Faulkner, M. Freyman, X. Lu, M. A. Worsley, J. Q. Lu and Y. Li, *Nano Lett.*, 2021, **21**, 3731–3737.
135 C. Cui, Y. Gao, J. Li, C. Yang, M. Liu, H. Jin, Z. Xia, L. Dai, Y. Lei, J. Wang and S. Wang, *Angew. Chem., Int. Ed.*, 2020, **59**, 7928–7933.
136 J. Yan, L. Miao, H. Duan, D. Zhu, Y. Lv, L. Li, L. Gan and M. Liu, *Chin. Chem. Lett.*, 2022, **33**, 2681–2686.
137 N. Li, X. Guo, X. Tang, Y. Xing and H. Pang, *Chin. Chem. Lett.*, 2022, **33**, 462–465.
138 L. Xuan, L. Chen, Q. Yang, W. Chen, X. Hou, Y. Jiang, Q. Zhang and Y. Yuan, *J. Mater. Chem. A*, 2015, **3**, 17525–17533.
139 M. Mansuer, L. Miao, D. Zhu, H. Duan, Y. Lv, L. Li, M. Liu and L. Gan, *Mater. Chem. Front.*, 2021, **5**, 3061–3072.
140 J. Chen, W. Xu, H. Wang, X. Ren, F. Zhan, Q. He, H. Wang and L. Chen, *J. Mater. Chem. A*, 2022, **10**, 21197–21250.
141 Y. Tang, S. Zheng, S. Cao, F. Yang, X. Guo, S. Zhang, H. Xue and H. Pang, *J. Colloid Interface Sci.*, 2022, **626**, 1062–1069.
142 Y. Cheng, X. Guo, Y. Xue and H. Pang, *Appl. Mater. Today*, 2021, **23**, 101048.
143 M. Wu, W. Zheng, X. Hu, F. Zhan, Q. He, H. Wang, Q. Zhang and L. Chen, *Small*, 2022, **18**, 2205101.
144 C. Long, L. Miao, D. Zhu, H. Duan, Y. Lv, L. Li, M. Liu and L. Gan, *ACS Appl. Energy Mater.*, 2021, **4**, 5727–5737.
145 L. Miao, X. Qian, D. Zhu, T. Chen, G. Ping, Y. Lv, W. Xiong, Y. Liu, L. Gan and M. Liu, *Chin. Chem. Lett.*, 2019, **30**, 1445–1449.
146 H. Lyu, J. Zhu, B. Zhou, H. Cao, J. Duan, L. Chen, W. Jin and Q. Xu, *Carbon*, 2018, **139**, 740–749.
147 Q. Huang, Y. Cong and Z. Xu, *Electrochim. Acta*, 2022, **426**, 140827.
148 X. Zheng, L. Miao, Z. Song, W. Du, D. Zhu, Y. Lv, L. Li, L. Gan and M. Liu, *J. Mater. Chem. A*, 2022, **10**, 611–621.
149 Q. Li, Z. Dai, J. Wu, W. Liu, T. Di, R. Jiang, X. Zheng, W. Wang, X. Ji, P. Li, Z. Xu, X. Qu, Z. Xu and J. Zhou, *Adv. Energy Mater.*, 2020, **10**, 1903750.
150 Z. Liu, A. Qin, K. Zhang, P. Lian, X. Yin and H. Tan, *Nano Energy*, 2021, **90**, 106540.
151 J. Li, K. Zhuang, Y. Mao, C. Liu, M. Pang and H. Li, *Carbon*, 2023, **201**, 449–459.
152 Y. Lu, Z. Li, Z. Bai, H. Mi, C. Ji, H. Pang, C. Yu and J. Qiu, *Nano Energy*, 2019, **66**, 104132.
153 H. Zhang, Q. Liu, Y. Fang, C. Teng, X. Liu, P. Fang, Y. Tong and X. Lu, *Adv. Mater.*, 2019, **31**, 1904948.
154 C. C. Hou, Y. Wang, L. Zou, M. Wang, H. Liu, Z. Liu, H. F. Wang, C. Li and Q. Xu, *Adv. Mater.*, 2021, **33**, 2101698.
155 H. Ma, H. Chen, M. Wu, F. Chi, F. Liu, J. Bai, H. Cheng, C. Li and L. Qu, *Angew. Chem., Int. Ed.*, 2020, **59**, 14541–14549.
156 L. Wang, M. Peng, J. Chen, X. Tang, L. Li, T. Hu, K. Yuan and Y. Chen, *ACS Nano*, 2022, **16**, 2877–2888.
157 L. Miao, Y. Lv, D. Zhu, L. Li, L. Gan and M. Liu, *Chin. Chem. Lett.*, 2023, **34**, 107784.
158 C. Huang, X. Zhao, Y. Xu, Y. Zhang, Y. Yang, A. Hu, Q. Tang, X. Song, C. Jiang and X. Chen, *ACS Sustainable Chem. Eng.*, 2020, **8**, 16028–16036.
159 L. Miao, J. Zhang, Y. Lv, L. Gan and M. Liu, *Chem.–Eur. J.*, 2023, **29**, DOI: **10.1002/chem.202203973**.
160 W. Jian, W. Zhang, X. Wei, B. Wu, W. Liang, Y. Wu, J. Yin, K. Lu, Y. Chen, H. N. Alshareef and X. Qiu, *Adv. Funct. Mater.*, 2022, **32**, 2209914.
161 S. Wu, Y. Chen, T. Jiao, J. Zhou, J. Cheng, B. Liu, S. Yang, K. Zhang and W. Zhang, *Adv. Energy Mater.*, 2019, **9**, 1902915.
162 J. Yin, W. Zhang, W. Wang, N. A. Alhebshi, N. Salah and H. N. Alshareef, *Adv. Energy Mater.*, 2020, **10**, 2001705.
163 Y. Shao, Z. Sun, Z. Tian, S. Li, G. Wu, M. Wang, X. Tong, F. Shen, Z. Xia, V. Tung, J. Sun and Y. Shao, *Adv. Funct. Mater.*, 2021, **31**, 2007843.

164 L. Zhou, Y. Yang, J. Yang, P. Ye, T. Ali, H. Wang, J. Ning, Y. Zhong and Y. Hu, *Appl. Surf. Sci.*, 2022, **604**, 154526.
165 P. Liu, W. Liu, Y. Huang, P. Li, J. Yan and K. Liu, *Energy Storage Mater.*, 2020, **25**, 858–865.
166 Z. Zhou, X. Zhou, M. Zhang, S. Mu, Q. Liu and Y. Tang, *Small*, 2020, **16**, 2003174.
167 Z. Song, L. Miao, L. Li, D. Zhu, L. Gan and M. Liu, *Carbon*, 2021, **180**, 135–145.
168 R. Yuksel, O. Buyukcakir, P. K. Panda, S. H. Lee, Y. Jiang, D. Singh, S. Hansen, R. Adelung, Y. K. Mishra, R. Ahuja and R. S. Ruoff, *Adv. Funct. Mater.*, 2020, **30**, 1909725.
169 H. Huang, R. Xu, Y. Feng, S. Zeng, Y. Jiang, H. Wang, W. Luo and Y. Yu, *Adv. Mater.*, 2020, **32**, 1904320.
170 Z. Liang, T. Qiu, J. Cheng, Y. Tang, Y. Wu, J. Shi, S. Gao and R. Zou, *Batteries Supercaps*, 2022, **5**, e20210026.
171 T. Chen, B. Cheng, G. Zhu, R. Chen, Y. Hu, L. Ma, H. Lv, Y. Wang, J. Liang, Z. Tie, Z. Jin and J. Liu, *Nano Lett.*, 2017, **17**, 437–444.
172 R. C. Cui, B. Xu, H. J. Dong, C. C. Yang and Q. Jiang, *Adv. Sci.*, 2020, **7**, 1902547.
173 Y. Gu, L. Miao, Y. Yin, M. Liu, L. Gan and L. Li, *Chin. Chem. Lett.*, 2021, **32**, 1491–1496.
174 Z. Liang, Y. Wu, J. Cheng, Y. Tang, J. Shi, T. Qiu, W. Li, S. Gao, R. Zhong and R. Zou, *Small*, 2021, **17**, 2100135.
175 L. Peng, H. Peng, L. Xu, B. Wang, K. Lan, T. Zhao, R. Che, W. Li and D. Zhao, *J. Am. Chem. Soc.*, 2022, **144**, 15754–15763.
176 Y. Tsao, H. Gong, S. Chen, G. Chen, Y. Liu, T. Z. Gao, Y. Cui and Z. Bao, *Adv. Energy Mater.*, 2021, **11**, 2101449.
177 Z. Song, L. Miao, H. Duan, L. Ruhlmann, Y. Lv, D. Zhu, L. Li, L. Gan and M. Liu, *Angew. Chem., Int. Ed.*, 2022, **61**, e202208821.